ELSEVIER

Geomorphology 40 (2001) 57–90

GEOMORPHOLOGY

www.elsevier.com/locate/geomorph

Peak discharge estimates of glacial-lake outburst floods and "normal" climatic floods in the Mount Everest region, Nepal

Daniel A. Cenderelli *, Ellen E. Wohl

Department of Earth Resources, Colorado State University, Fort Collins, CO 80225, USA

Received 9 March 2000; received in revised form 8 January 2001; accepted 13 January 2001

Abstract

Glacial-lake outburst floods (GLOFs) in the Mount Everest region of Nepal on 3 September 1977 and 4 August 1985 dramatically modified channels and valleys in the region by eroding, transporting, and depositing large quantities of sediment for tens of kilometers along their flood routes. Prior to this research, the GLOF discharges had not been determined and the hydrology of "normal" climatic floods (SHFFs: seasonal high flow floods) was not known. A one-dimensional step-backwater flow model was utilized, in conjunction with paleostage indicators, to estimate the peak discharges of the GLOFs and SHFFs and to reconstruct the hydrology and hydraulic conditions of the GLOFs at 10 reaches and SHFFs at 18 reaches. The most reliable GLOF and SHFF peak discharge estimates were upstream from constrictions where there was critical-depth control.

The peak discharge of the 1977 GLOF at 8.6 km from the breached moraine was approximately 1900 m^3/s. At 7.1 km downstream from the breached moraine, the 1985 GLOF discharge was estimated at 2350 m^3/s. At 27 km downstream from the breached moraine, the 1985 GLOF attenuated to an estimated discharge of 1375 m^3/s. The peak discharges of SHFFs ranged from 7 to 205 m^3/s and were positively correlated with increasing drainage area. The GLOF discharges were 7 to 60 times greater than the SHFF discharges with the greatest ratios occurring near the breached moraines. The downstream decline in the ratio between the GLOF discharge and SHFF discharge is the result of the downstream attenuation of the GLOF and the increased discharge of the SHFF because of increased contributing drainage area and the increased effects of monsoonal precipitation at lower elevations. © 2001 Elsevier Science B.V. All rights reserved.

Keywords: Glacial-lake outburst floods; Seasonal high flow floods; Paleoflood hydrology; Step-backwater modeling; Peak discharge estimates; Mount Everest

1. Introduction

The Mount Everest region of Nepal experienced two extraordinary floods on 3 September 1977 and 4 August 1985 when glacial lakes, situated immediately downstream from alpine glaciers, breached their moraine dams. Both glacial-lake outburst floods (GLOFs) dramatically modified channel and valley morphology for tens of kilometers downstream from the source area (Fig. 1). Although the discharges of both GLOFs have been described as several orders of magnitude larger than typical annual floods in the region, the peak discharges of the 1977 and 1985

* Corresponding author. Department of Geological Sciences, University of Alabama, Box 870338, Tuscaloosa, AL 35487-0338, USA.

0169-555X/01/$ - see front matter © 2001 Elsevier Science B.V. All rights reserved.
PII: S0169-555X(01)00037-X

GLOFs along the upper segments of their flood route had not been systematically quantified prior to the research described in this paper. In the Mount Everest region, annual peak discharges are caused by the

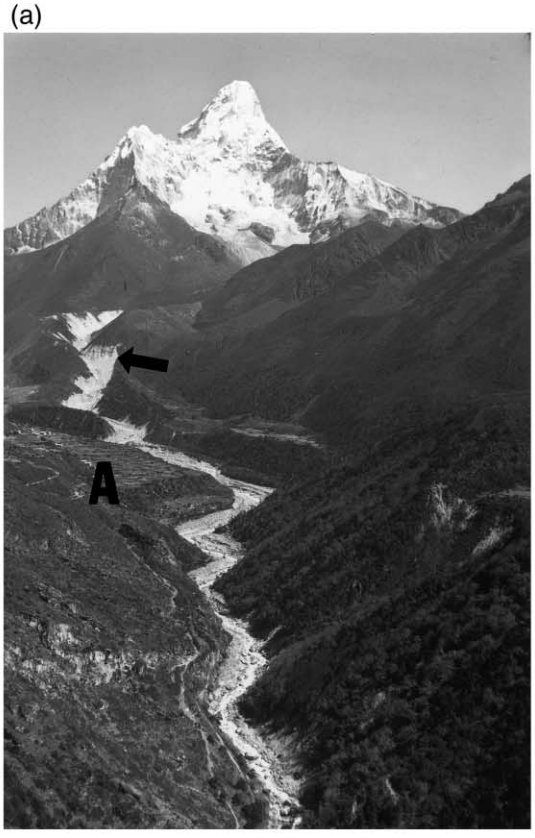

combination of seasonal snowmelt, glacier meltwater, and monsoonal precipitation (in this paper, these floods are referred to as seasonal high flow floods, SHFFs). However, the magnitude, duration, and timing of SHFFs are poorly understood because streams in the region have never been gaged.

In the absence of gaging stations or direct stream measurements, paleoflood hydrology techniques can be used to estimate the peak discharge of floods. Paleoflood hydrology is the study of floods that occurred in the absence of direct measurements or prior to when hydrological records were collected from a given stream (Baker, 1987; Jarrett, 1990). Paleoflood hydrology studies in ungaged watersheds can provide invaluable information for water-resource managers, hydrologists, and fluvial geomorphologists concerned with past and potential flooding in an area. Additionally, geomorphologists assessing fluvial processes and the geomorphic effects of extreme floods require accurate discharge estimates in order to calculate local flow hydraulics. Paleoflood hydrology identifies and uses erosional and depositional features produced by past floods to delineate the probable water-surface elevation of the floods and to estimate the magnitude of those floods. Evidence left by a flood is referred to as paleostage indicators (PSIs) and includes scour lines, scars on vegetation, silt lines, debris accumulations, slackwater sediments, and boulder bars. Nonflooded surfaces along the flood route can also be considered paleostage indicators. Where there are PSIs along a given channel reach, the flood discharge can be reconstructed by calculating water-surface profiles using the step-backwater method in conjunction with the PSIs. Numerous studies in a variety of environments have effectively demonstrated the use of the step-backwater method to estimate the peak discharges and flow hydraulics of ungaged floods (e.g., Ely and Baker, 1985; Jarrett and Malde, 1987; Webb et al., 1988; Wohl, 1992a, 1992b, 1995; O'Connor, 1993; O'Connor and Baker, 1992; O'Connor et al., 1986; Rathburn, 1993; Grimm et al., 1995; House and Pearthree, 1995; Waythomas et al., 1996; Benito, 1997). Of these studies, several used the step-backwater method to reconstruct floods from dam failures, such as the Pleistocene Lake Missoula glacier-dam failure flood(s) (O'Connor and Baker, 1992; Benito, 1997), the Pleistocene Lake Bonneville flood (Jarrett and Malde, 1987; O'Connor, 1993), and Aniakchak Caldera flood (Waythomas et al., 1996).

Prior to the work described here, no studies have quantified the annual peak discharges of SHFFs on streams in the Mount Everest region or systematically quantified the peak discharges of the 1977 and 1985 GLOFs along their flood routes. The purposes of this paper are to (i) demonstrate the application of the step-backwater method, used in conjunction with geomorphic evidence, in estimating the magnitude of previously unquantified GLOFs and SHFFs in the Mount Everest region of Nepal and (ii) improve the understanding of flood hydrology in this remote, mountainous region. For the 1977 and 1985 GLOFs, multiple reaches along the GLOF were selected to assess the downstream changes in the discharge magnitude of the flood wave. The SHFFs characterize the hydrology of "normal" climatic floods in the region and provide a baseline to which the GLOF discharges can be compared.

2. Study area

2.1. Geology and geomorphology

The Mount Everest region is located in eastern Nepal (Fig. 2). The area is underlain primarily by Precambrian gneiss and granite (Vuichard, 1986), lies within the High Himalaya Physiographic Province, and is characterized by extremely high relief. The four major valleys in the area, Bhoti Kosi,

Fig. 1. (a) Upstream view of the Imja Khola valley (foreground) and the Nare Khola valley (arrow) showing the erosional and depositional effects of the 1977 GLOF. The river valley bottom in the foreground is approximately 50 to 70 m wide. The stone wall pastures on the right valley margin (A) are the lower outskirts of the village Pangboche and the mountain in the background is Ama Dablam. (b) Upstream view of the Bhoti Kosi valley showing the erosional and depositional effects of the 1985 GLOF. This segment of the river valley is approximately 16 km downstream from the breached moraine. The village of Thamo (A) is located on a glaciofluvial terrace along the left valley margin. A nearly completed hydroelectric dam (B) that was located on the fan was destroyed by the 1985 GLOF.

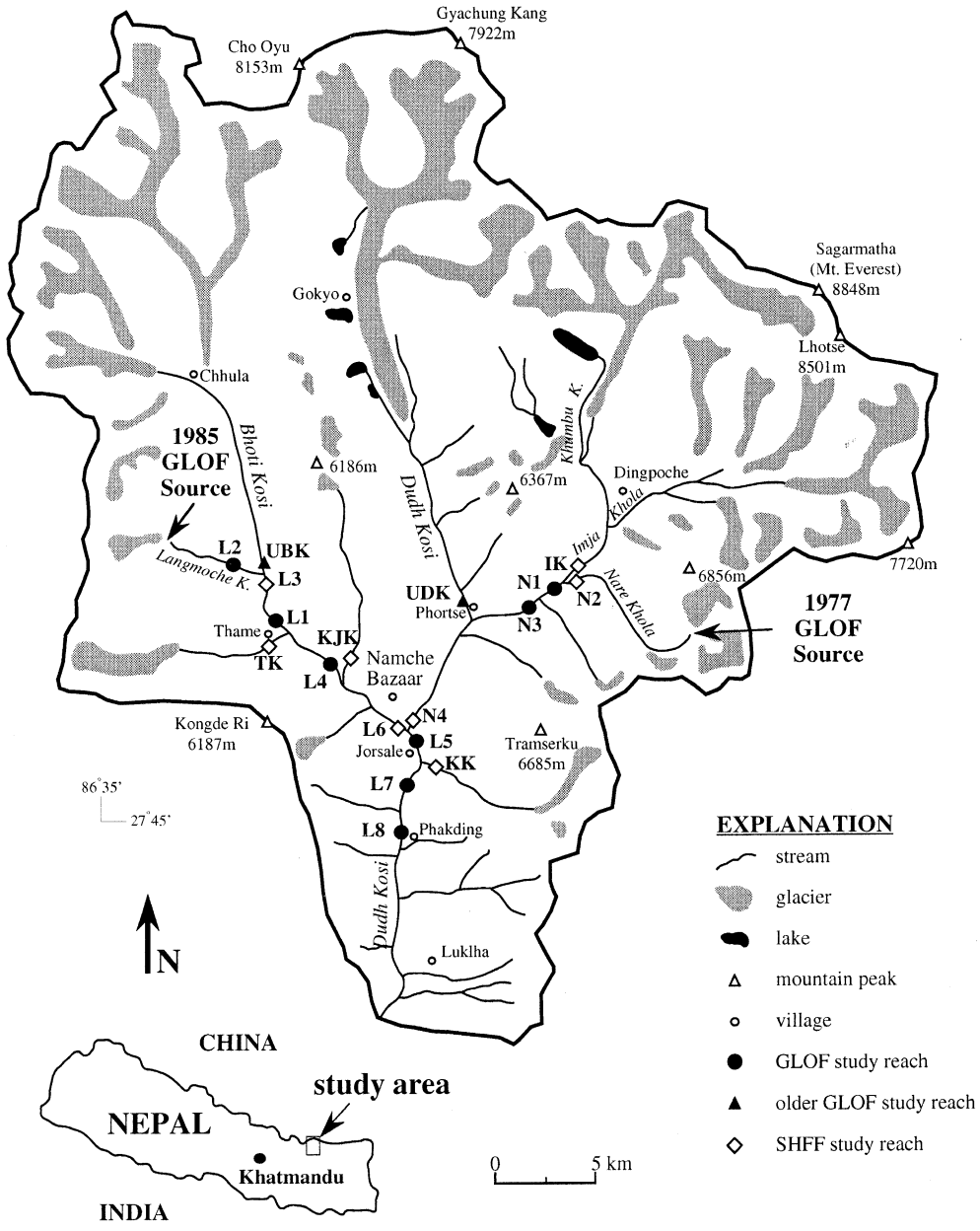

Fig. 2. Map of the study area showing the locations of study reaches for the 1977 GLOF, 1985 GLOF, older GLOFs, and tributaries. N designates 1977 study reaches, L designates 1985 study reaches. For the older GLOF study reaches: UBK = upper Bhoti Kosi and UDK = upper Dudh Kosi. For the tributary study reaches: IK = Imja Khola, KJK = Kyajo Khola, KK = Kyashar Khola, and TK = Thame Khola.

Dudh Kosi, Imja Khola, and Khumbu Khola, are deeply incised with valley floors 4000 m lower than the surrounding mountains (Fig. 1). The Nepalese term "Kosi" indicates a major stream or large river, whereas the term "Khola" indicates a smaller stream. Valleys at elevations higher than 3400 to 3600 m

were glaciated during the Pleistocene (Fushimi, 1977, 1978), are distinctly U-shaped, and have boundaries consisting of bedrock, coarse-grained colluvium, or coarse-grained glaciofluvial sediment. Below 3400 to 3600 m, valleys are V-shaped and have boundaries consisting primarily of bedrock and secondarily terraces comprised of coarse-grained sediment. Alpine glaciers are typically present at elevations above 4500 m and have been, for the most part, in retreat from their Little Ice Age maximum positions, creating numerous moraine-and glacier-dammed lakes (Mayewski and Jeschke, 1979; Fushimi et al., 1985).

2.2. Climate and hydrology

Hydrology in the study area is strongly influenced by monsoonal precipitation and late spring/early summer snowmelt. Eighty percent of the total annual precipitation occurs between June and September with the most intense precipitation typically occurring from mid-July to mid-August (Ageta, 1976; Brower, 1991). The high mountain topography, however, creates a rain-shadow effect that reduces the intensity and amount of monsoonal precipitation with increasing elevation (Ageta, 1976; Zimmermann et al., 1986). For example, from June to September 1974 in the Mount Everest region, the total precipitation was 1100 mm at 2700 m, 685 mm at 3900 m, and 428 mm at 4400 m (Ageta, 1976). Although not quantified, discharge in the study area is characterized by low flow from late fall to early spring and high flow from late spring to early fall because of the combined runoff produced by snowmelt, glacier meltwater, and monsoonal precipitation.

2.3. The 1977 and 1985 glacial-lake outburst floods

On 3 September 1977, a series of ice-cored moraine dams failed below the Nare Glacier, sending a flood surge down the Nare Khola, Imja Khola, and Dudh Kosi valleys (Fig. 2) (Buchroithner et al., 1982; Fushimi et al., 1985; Zimmermann et al., 1986). This flood caused extensive erosion and deposition for 35 km downstream from the source area, destabilized valley side slopes, and destroyed bridges and trails (Fig. 1a) (Ives, 1986; Zimmermann et al., 1986). Based on a field survey, the volume of water released by the lake was estimated to be 500,000 m^3 (Fushimi et al., 1985), although Buchroithner et al. (1982) reported a lake volume of 5,000,000 m^3 based on remote sensing imagery. At a gaging station located 90 km from the breached moraine, the 1977 GLOF had an estimated peak discharge of 800 m^3/s that lasted about 1 h and a total flood duration of approximately 6 h (Fig. 3).

On 4 August 1985, a moraine-dammed lake located below the Langmoche Glacier failed when an ice avalanche from the glacier plunged into the lake, triggering a surge wave that breached the moraine (Vuichard and Zimmermann, 1986, 1987; Ives,

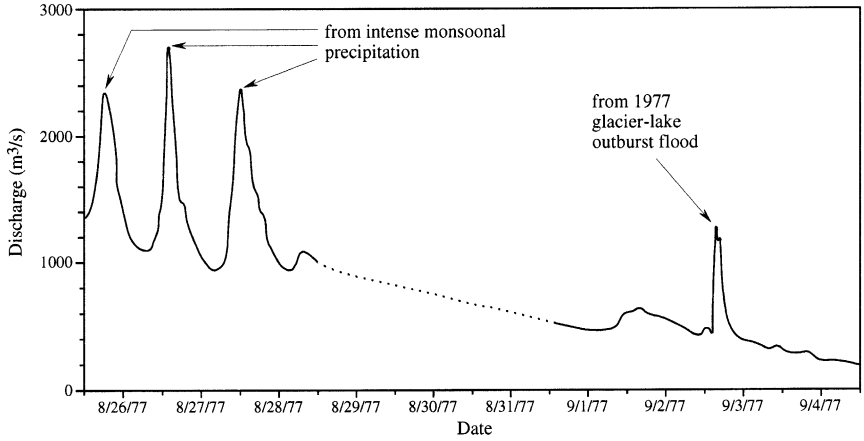

Fig. 3. Discharge hydrograph of the Dudh Kosi at the Rabuwa Bazar gaging station from 26 August 1977 to 4 September 1977. The increase in discharge of the Dudh Kosi on 3 September 1977 is due to the 1977 GLOF that originated 90 km upstream from the gaging station (modified from Zimmermann et al., 1986).

1986). The volume of water released was estimated to be 5,000,000 m^3 (Ives, 1986; Vuichard and Zimmermann, 1986, 1987). The gaging station that recorded the discharge of the 1977 GLOF was not in operation at the time of the 1985 GLOF. Vuichard and Zimmermann (1987) estimated that the 1985 outburst flood had a peak discharge of 1600 m^3/s at a distance of 2 km from the breached moraine. Based

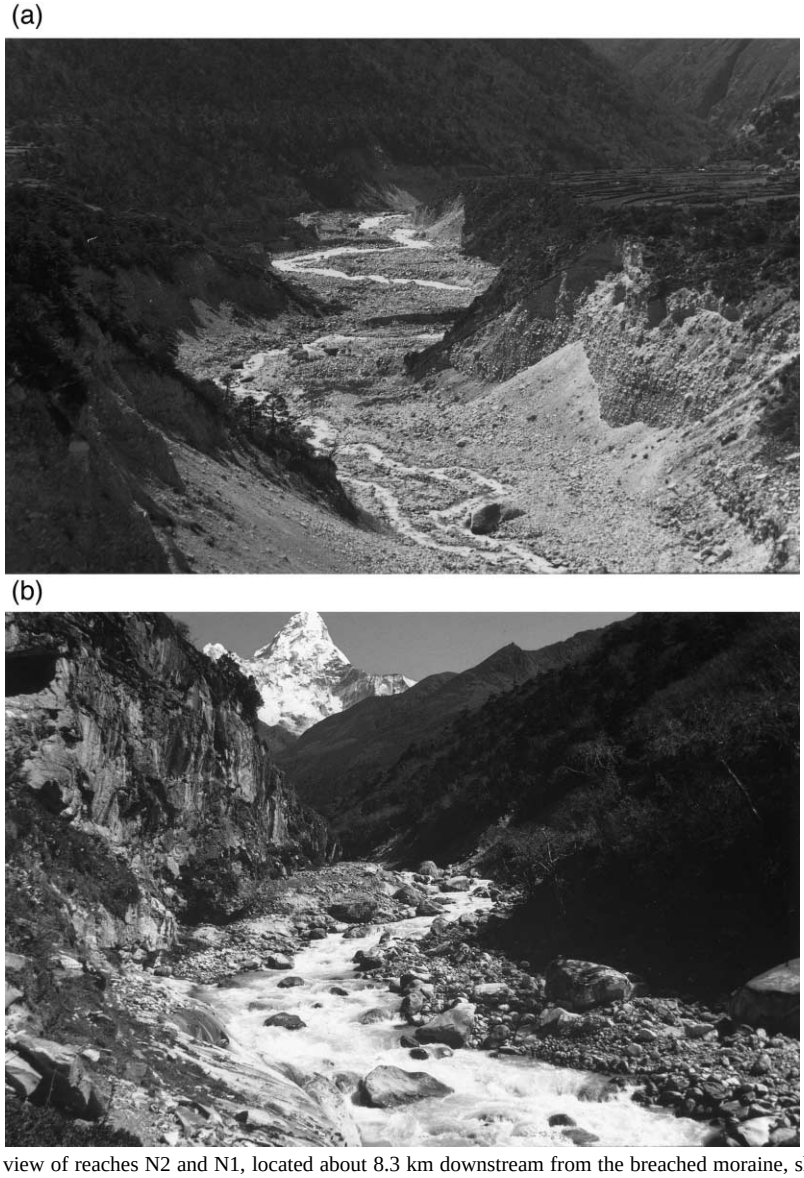

Fig. 4. (a) Downstream view of reaches N2 and N1, located about 8.3 km downstream from the breached moraine, showing the geomorphic effects of the 1977 GLOF. Reach N1 is located on the Imja Khola (background), approximately 500 m downstream from reach N2. Note the extensive erosion of the coarse-grained glaciofluvial terraces along the valley side margins and deposition of cobbles and boulders across the valley bottom. Valley in the background is approximately 125 m wide and the valley in the foreground is approximately 60 m wide. (b) Upstream view of reach N3 showing the geomorphic effects of the 1977 GLOF. Reach N3 is located on the Imja Khola at approximately 11.5 km downstream from the breached moraine. The valley is relatively narrow, ranging in width between 30 and 45 m, with valley boundaries consisting primarily of bedrock and coarse-grained glaciofluvial terraces or colluvium.

on discussions with residents at various villages along the GLOF route, Vuichard and Zimmermann (1987) estimated that the GLOF peak discharge had a duration of approximately 1 h and that the total GLOF duration was between 6 and 8 h. The resulting flood caused considerable erosion and deposition for 40 km along the Langmoche Khola, Bhoti Kosi, and Dudh Kosi (Figs. 1b and 2) resulting in the destruction of several bridges, tens of houses, and a nearly completed hydroelectric power plant (Ives, 1986; Vuichard and Zimmermann, 1987). Using photographs taken before and after the flood, Vuichard and Zimmermann (1987) estimated that approximately 3,000,000 m^3 of sediment were eroded and deposited along the flood route; approximately 70% of this total occurred in the first 16 km of the flood route.

The 1977 and 1985 GLOFs produced an assortment of erosional and depositional features along their flood routes (Figs. 4 and 5). Erosion of valley slopes and valley bottoms was the predominant geomorphic process in narrow, steep valleys with boundaries comprised of coarse, unconsolidated sediment (Figs. 6 and 7). Deposition was dominated by coarse sediment (primarily boulder-, cobble-, and pebble-size particles) and typically occurred in wider, less steep reaches across the entire valley bottom where flow energy was reduced and flow was diverging. Deposition typically occurred at locations where the channel and/or valley widened, upstream and downstream of obstructions, and along the margins of channel bends (Figs. 6 and 7). The deposits produced by the 1977 and 1985 GLOFs were depositional macroforms (Baker, 1978, 1984; Church and Jones, 1982) and consisted primarily of expansion bars and longitudinal bars and secondarily of point bars, pendant bars, and imbricate clusters (Figs. 6 and 7). Fine-grained sedimentation was minimal along the 1977 and 1985 GLOF routes, but did occur in areas upstream of constrictions where ponding occurred or along channel and valley margins where flow energy was reduced and/or recirculating (Fig. 7A, C and F). The sedimentologic characteristics of the 1977 and 1985 GLOF deposits have been described elsewhere by Cenderelli (1998), Cenderelli and Cluer (1998), and Cenderelli and Wohl (1998). In general, along the upper 10 km of the 1977 GLOF route and the upper 16 km of the 1985 GLOF route, erosion and deposition were more pronounced than below these distances from the breached moraines (compare Fig. 4a to b, Fig. 5a and b to 5c and d, Fig. 6a to b and Fig. 7A–C to D–F).

2.4. Evidence of older, previously undocumented glacial-lake outburst floods

During field reconnaissance of the upper Bhoti Kosi and upper Dudh Kosi drainages, cobble-boulder deposits located adjacent to and 3 to 5 m above the present-day channel on the surface of lower glaciofluvial terraces were identified (Figs. 2 and 8). These deposits were interpreted to have been deposited by GLOFs of an unknown age; however, the heavily lichen-encrusted cobbles and boulders indicate that these deposits are considerably older than the 1977 and 1985 GLOFs. The upper Bhoti Kosi GLOF deposits appear to be younger than the upper Dudh Kosi GLOF deposits (compare Fig. 8a to b), but considerably older than the 1977 and 1985 GLOFs. The older GLOF deposits are clast-supported and composed primarily of cobbles and boulders that are moderately imbricated. No attempt was made to trace the GLOF deposits to the source area.

3. Methods

3.1. Selection of study reaches

Ten reaches along various streams in the study area were selected to estimate the peak discharges of both GLOFs and SHFFs using the step-backwater method (Fig. 2). Two reaches were studied along the 1977 GLOF route (reaches N1 and N3), six reaches were studied along the 1985 GLOF route (reaches L2, L1, L4, L5, L7, and L8), and two reaches were studied where evidence of older GLOFs were identified (reaches UDK and UBK). Eight other reaches (TK, IK, KYK, KJ, L3, L6, N2, and N4) were selected to estimate the peak discharge of SHFFs for comparative purposes (Fig. 2). The physical characteristics of the study reaches are summarized in Table 1. The criteria used to select these reaches were (i) accessibility to the stream, (ii) relatively straight and uniform or gradually narrowing reaches

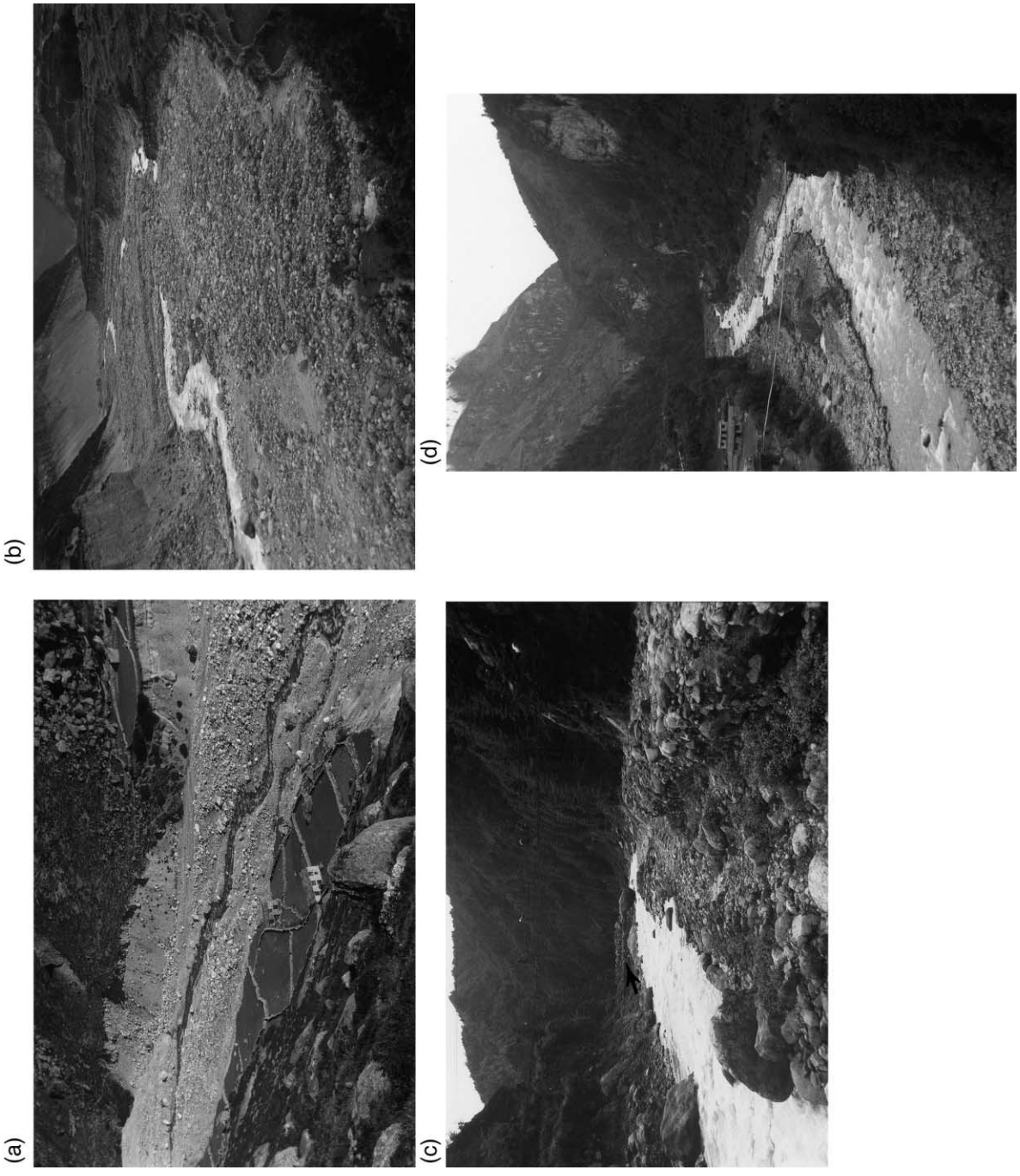
(a)
(b)
(c)
(d)

so that the floods could be accurately modeled using the step-backwater method, and (iii) the presence of multiple paleostage indicators produced by the GLOF and SHFF to delineate the water-surface elevation of the floods. Although reaches N2, N4, L3, and L6 are located along the 1977 or 1985 GLOF routes, the GLOF peak discharges were not calculated at these reaches because they were not appropriate for modeling using the step-backwater method. At reach N2, GLOF deposits were interpreted to be fluvially reworked, noncohesive, sediment gravity-flow deposits. At reach N4, there was no geomorphic evidence of the 1977 GLOF. Reaches L3 and L6 are located in hydraulic settings that caused flow during the GLOF to be rapidly varied. Although reaches N2, N4, L2, and L6 were not well suited for modeling the GLOF using the step-backwater model, they were appropriate for modeling the SHFFs.

3.2. Characterizing channel and valley geometry

To accurately estimate discharge using the step-backwater method, the channel/valley geometry must be adequately characterized and representative of the channel/valley conditions at the time of the flood (Bailey and Ray, 1966; O'Connor and Webb, 1988). In this study, reaches were surveyed using standard transit-stadia rod techniques to characterize the channel and valley geometry. Depositional features, erosional features, and/or nonflooded surfaces were identified, surveyed, and mapped at each cross-section to constrain the flood stage of the GLOFs and SHFFs. Cross-sections were surveyed perpendicular to the assumed flow direction, placed at locations that best characterized the channel geometry of the modeled reaches, and placed at locations so that channel geometry changes between successive cross-sections were relatively gradual (Figs. 6 and 7). Along the 1977 and 1985 outburst-flood routes, the surveyed channel and valley geometry were assumed to represent the geometry of the channel and valley during peak flow. Although segments of the modeled reaches experienced considerable erosion and deposition during the GLOFs (in particular, reaches N1, L2, L3, L1, and L4), these geomorphic processes are assumed to have occurred in close proximity to peak flow and were minimal during the receding limb of the GLOFs. Large quantities of coarse-grained sediment introduced to the channel by the GLOFs, and SHFFs are incapable of reworking that sediment and modifying the geometry of the main channel (Cenderelli and Wohl, in review).

3.3. Paleostage indicators used in this study

At all of the study sites, multiple paleostage indicators of the GLOFs and SHFFs were identified and surveyed at numerous cross-sections along a given modeled reach. Upper surfaces of boulder and cobble bars, scour lines, and the lowest elevation of non-flooded surfaces were used to define the peak stages of the 1977 and 1985 GLOFs, as well as the older GLOFs identified in the study area. Upper surfaces of boulder and cobble bars were assumed to represent a minimum peak stage of the outburst floods.

Fig. 5. (a) Cross valley view of the middle portion of reach L2 showing the geomorphic effects of the 1985 GLOF. The valley in the center of the photo is approximately 110 m wide and the flow direction is from left to right. Reach L2 is located on the Langmoche Khola, approximately 7.1 km downstream from the breached moraine. (b) Downstream view of middle segment of reach L1, which is located on the Bhoti Kosi approximately 11 km downstream from the moraine breached in 1985, showing the geomorphic effects of the GLOF. In the foreground the valley width ranges from 150 to 225 m. Deposition was the primary geomorphic process as expansion bars comprised primarily of cobbles and boulders were deposited across the valley bottom. (c) Downstream view of reach L5, which is located approximately 22.1 km downstream from the moraine breached in 1985 along the Dudh Kosi near the village of Jorsale. The valley slopes consist of near vertical bedrock walls, coarse-grained colluvium, or coarse-grained glaciofluvial terraces. In the foreground on the right bank and background on the left bank (arrow), note the bank erosion and deposition of cobbles and boulders on the surface of the lower Glaciofluvial terraces. The foot bridge extending across the valley is approximately 70 m long. (d) Upstream view of reach L8 along the 1985 GLOF route, which is located on the Dudh Kosi near the village of Phakding approximately 26.7 km downstream from the breached moraine. The foot bridge extending across the valley is approximately 80 m long. The valley slopes consist of near vertical bedrock walls, coarse-grained colluvium, or coarse-grained glaciofluvial terraces. Erosion of valley side slopes was minimal, but the surfaces of the glaciofluvial terrace were eroded. Deposition was minimal and consisted primarily of longitudinal bars comprised of cobbles and boulders deposited on the surfaces of lower glaciofluvial terraces.

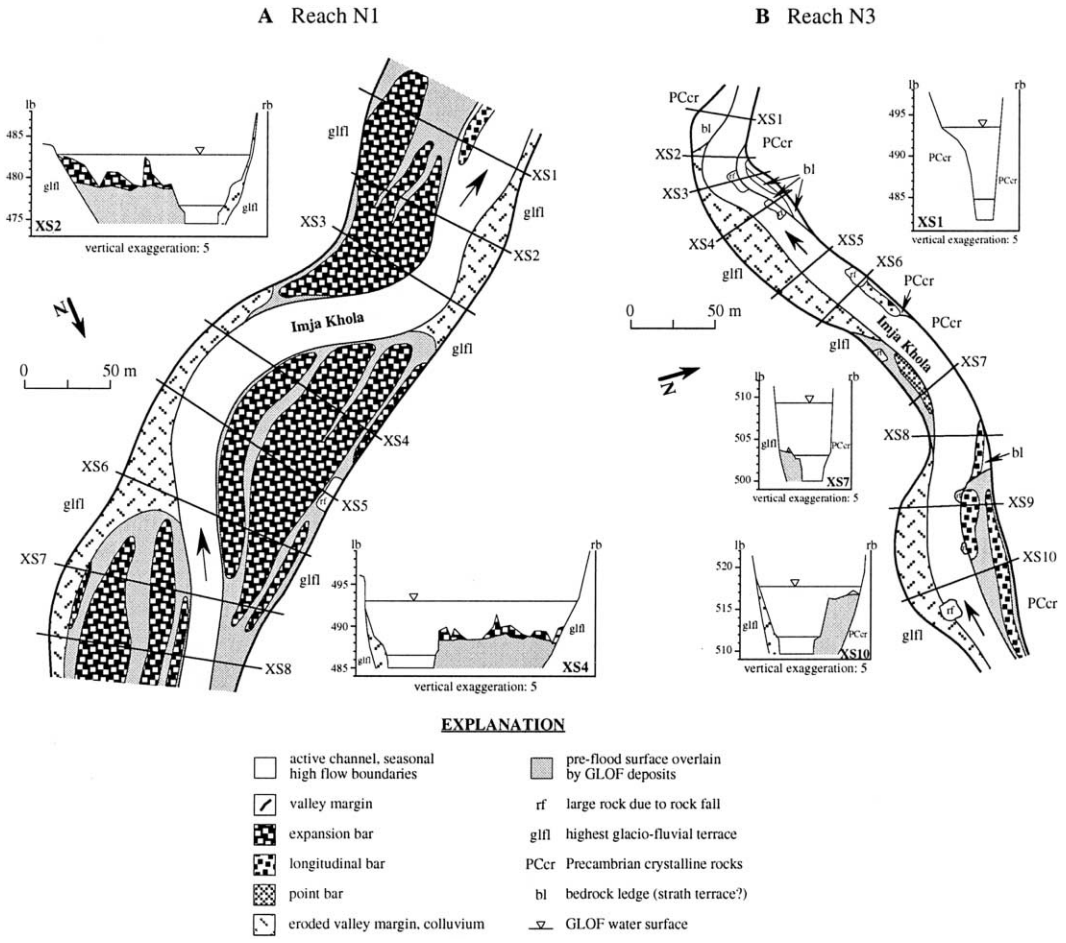

Fig. 6. Geomorphic maps of reach N1 (A) and reach N3 (B) showing the distribution of erosional and depositional features produced by the 1977 GLOF.

However, Stewart and LaMarche (1967), Costa (1983), and Carling (1987) documented the surface of longitudinal bars at the flood-water surface or just below the water surface. Additionally, Jarrett (in review) conducted a systematic study of floods in the western USA, showing that the top of boulder bars may be just below the water surface, at the water surface, or protrude above the water in some cases. Thus, the top of cobble-boulder bars in this study may also represent the maximum peak stage of the GLOFs or, in some instances, slightly overestimate the peak stage of the GLOFs.

Scour lines and nonflooded surfaces identified along the study reaches were considered to represent the maximum peak stage of the outburst flood. Scour lines may be considerably higher than the actual water surface if undercutting of the side slope caused the surface above the water surface to fail, so caution should be exercised when using this type of PSI. Nonflooded surfaces, such as alluvial fans and glaciofluvial terraces, were identified as such if sediment was not deposited on these surfaces and the surfaces were not eroded during the GLOF. However, water can overtop a surface without depositing sediment or eroding that surface. Thus, nonflooded surfaces do not absolutely delineate the maximum elevation of a given flood, but were probably a reasonable assumption in most situations.

Streams in the study area have relatively high concentrations of sediment in suspension because the

headwaters of most streams are occupied by glaciers and underlain by glacial sediment (Fig. 2). During the field season, the streams had a distinct, milky-white-gray color. Along the cobble-boulder margins of the main channel, a well-defined powdery-white-gray colored silt-clay line is present and was used to delineate the water-surface elevation of the SHFFs. The silt-clay PSIs identified at reaches N1, N2, N3, and N4 represent the largest SHFF that has occurred since the GLOF in 1977, whereas the silt-clay PSIs identified at reaches L2, L3, L1, L4, L6, L5, L7, and L8 represent the largest SHFF that has occurred since the GLOF in 1985. For the older GLOF and tributary study reaches, the ages of the SHFFs that produced the silt-clay PSIs are unknown.

3.4. Discharge calculations

3.4.1. Step-backwater modeling

The computer program HEC-RAS (Hydrologic Engineering Center-River Analysis System), developed by the Hydrologic Engineering Center of the U.S. Army Corps of Engineers (1995), was used to perform the step-backwater calculations and estimate the peak discharges of the SHFFs and GLOFs. The hydraulic theory of step-backwater analysis and its application to natural channels have been discussed in detail by Chow (1959), Bailey and Ray (1966), Davidian (1984), Hoggan (1989), O'Connor (1993) and O'Connor and Webb (1988) and will only be briefly reviewed here.

The step-backwater method calculates a one-dimensional, energy-balanced, water-surface profile that is a function of discharge, channel roughness, and channel geometry (Chow, 1959; Bailey and Ray, 1966; Davidian, 1984; Hoggan, 1989; O'Connor, 1993; O'Connor and Webb, 1988; Hydrologic Engineering Center, 1995). Flow can be modeled as subcritical, supercritical, or both subcritical and supercritical (mixed flow regime). For subcritical flow, the step-backwater calculations begin at the furthest downstream cross-section and proceed upstream; whereas for supercritical flow, step-backwater calculations begin at the furthest upstream cross-section and proceed downstream. To perform the step-backwater calculations for subcritical flow, a starting water-surface elevation needs to be estimated at the furthest downstream cross-section by assuming either (i) a known water-surface elevation defined by a PSI, (ii) critical depth (which is calculated by iteratively determining the water-surface elevation at the cross-section so that the specific energy is at a minimum), or (iii) normal depth (in which the energy slope should be entered; however, bed slope can be substituted for energy slope because these slopes are equal for normal depth or uniform flow conditions). A known water-surface elevation is selected if a PSI has been identified at the furthest downstream cross-section. Critical depth is selected at channel transitions, such as abrupt steepening in slope or narrowing of the channel/valley that causes flow to change from subcritical to supercritical flow. Immediately upstream from the channel transition, flow is critical and the total energy head is at a minimum. The critical depth or critical water-surface elevation can be determined by the equation:

$$H = WS + \alpha_2 v_2^2 / 2g, \quad (1)$$

where H is the total energy head, WS is the water surface elevation, and $\alpha_2 v_2^2/2g$ is the velocity head. Solving Eq. (1) is an iterative procedure (calculated in the HEC-RAS program) in which WS values are assumed and changed until a minimum H value is obtained. Normal depth is selected if the known water-surface elevation or critical depth criteria are not met. Normal depth is calculated using Manning's equation. If normal depth is selected, the user must enter the energy slope, which can be approximated by entering the channel slope at the furthest downstream cross-section. Regardless of the initial starting water-surface elevation, the water-surface profile will typically converge to a single profile for a specified discharge if the step-backwater calculations are carried upstream for an adequate distance, typically three or four cross-sections (Bailey and Ray, 1966; O'Connor and Webb, 1988).

For a specified discharge and assumed friction and form energy losses, the step-backwater method iteratively calculates an energy-balanced, water-surface elevation between the surveyed cross-sections. The elevation of the PSIs at cross-sections along a surveyed reach are then compared to the computed water-surface elevation at the respective cross-sections. The water-surface profile is adjusted

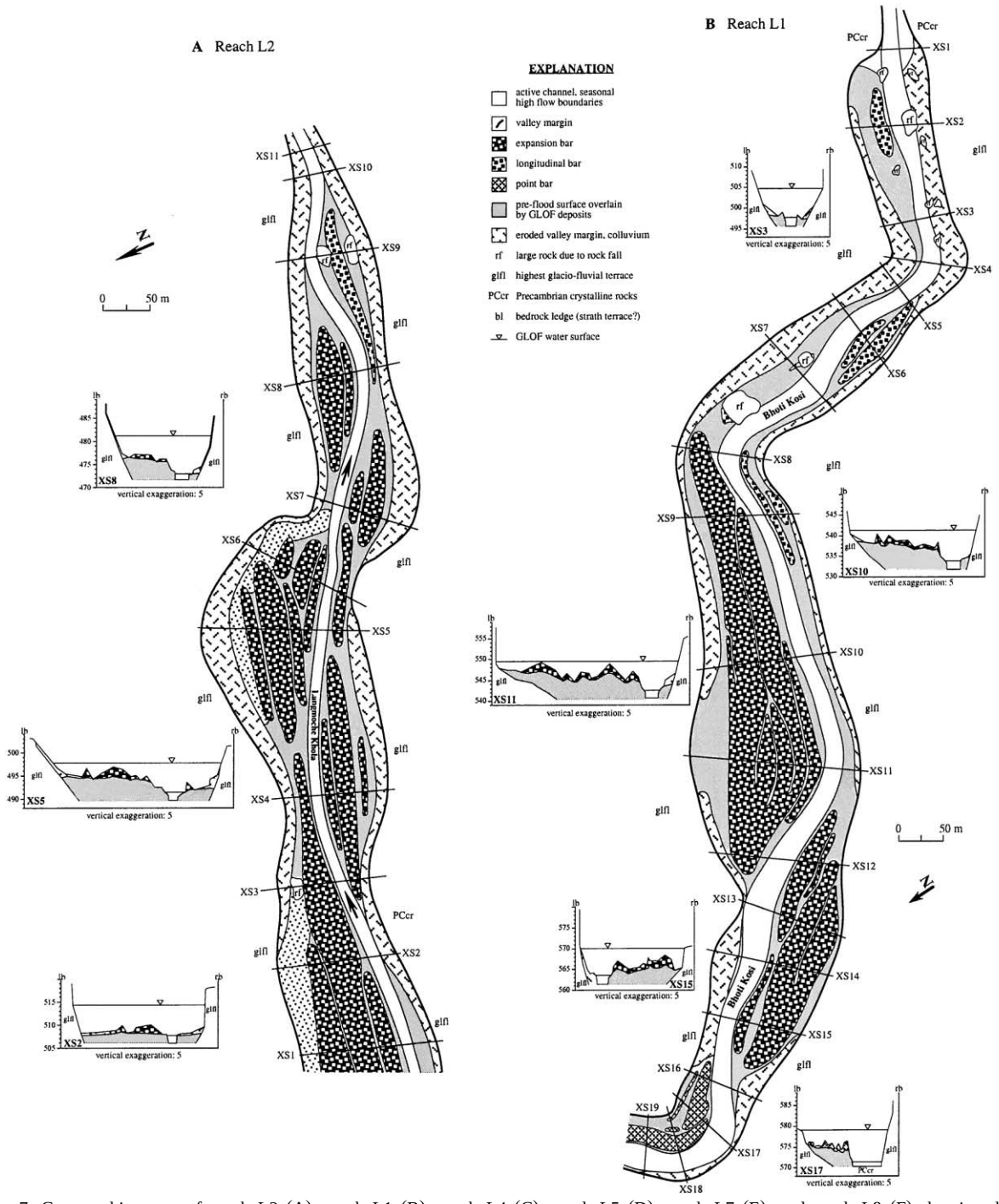

Fig. 7. Geomorphic maps of reach L2 (A), reach L1 (B), reach L4 (C), reach L5 (D), reach L7 (E), and reach L8 (F) showing the distribution of erosional and depositional features produced by the 1985 GLOF.

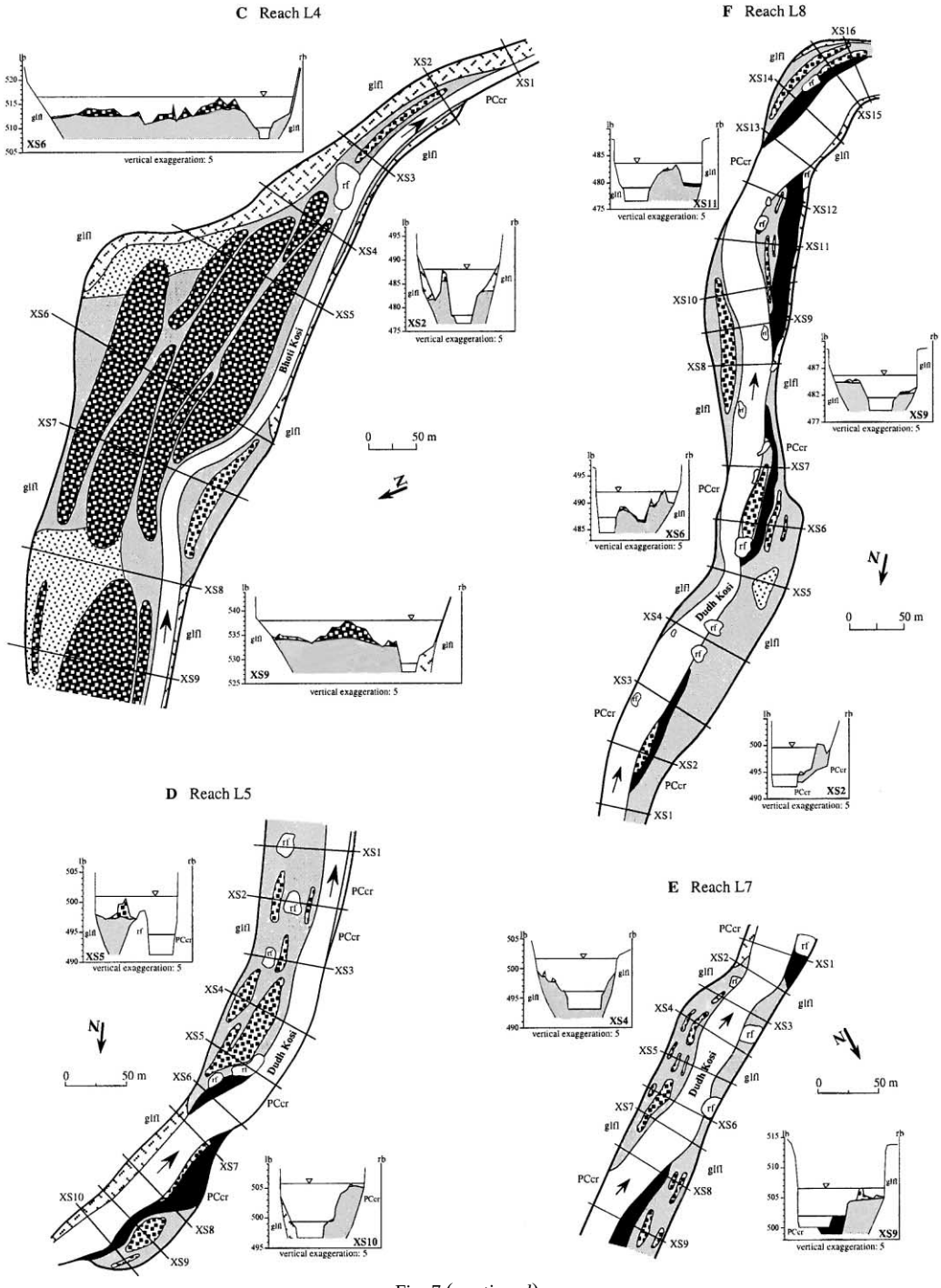

Fig. 7 (*continued*).

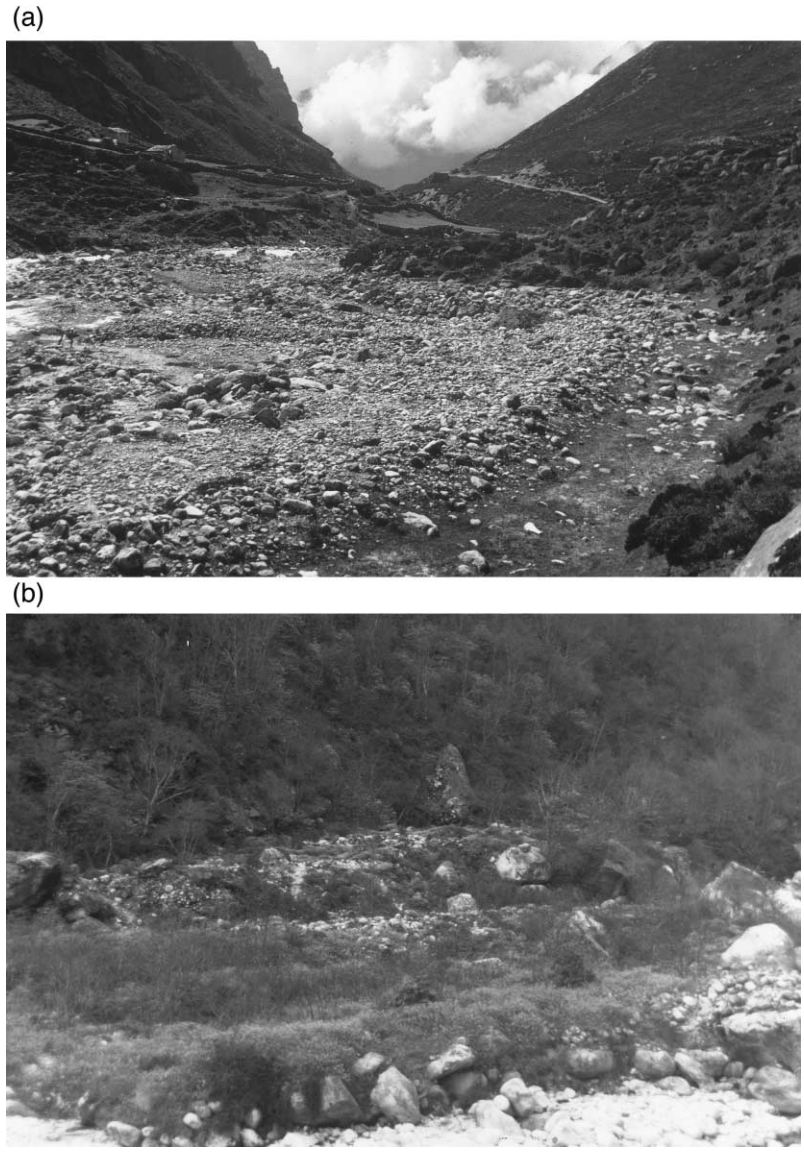

Fig. 8. (a) Downstream view of the older GLOF deposits identified along the upper Bhoti Kosi (reach UBK). The valley width ranges between 50 and 70 m. Although not easily seen in the photograph, the cobbles and boulders are encrusted by lichens. (b) Side view of an older GLOF deposit identified along the upper Dudh Kosi (reach UDK). Field of view is 60 m wide.

by varying discharge until the computed water-surface profile best matches the PSIs at the modeled reach.

When applying the step-backwater method to natural channels, the basic assumptions are that (i) flow is relatively steady or constant along the surveyed reach, (ii) flow is gradually varied between successive cross-sections, (iii) flow is one dimensional, (iv) slopes are less than 10%, and (v) the energy slope between successive cross-sections is constant across the cross-section (Bailey and Ray, 1966; Davidian, 1984; O'Connor and Webb, 1988; Hoggan, 1989;

Table 1
Summary of survey parameters and Manning's n coefficients for the study reaches of the GLOFs and SHFFs

Study reach[a]	Distance from breached moraine (km)	Reach elevation (m)	Drainage area (km^2)	Reach length (m)	Number of cross sections	Average gradient	Initial channel n for GLOF[b]	Adjusted channel n for GLOF	Initial overbank n for GLOF[b]	Channel n for SHFF[c]
1977 GLOF										
N1	8.6	3840	339	385	8	0.070	0.100	0.160	0.300	0.110
N3	11.5	3790	365	340	10	0.087	0.100	0.140	0.200	0.120
1985 GLOF										
L2	7.1	4080	41	1000	10	0.053	0.100	0.125	0.300	0.105
L1	10.9	3710	295	1565	19	0.060	0.100	0.140	0.300	0.105
L4	15.6	3440	356	775	9	0.071	0.100	0.140	0.300	0.110
L5	22.1	2770	1093	490	10	0.033	0.100	0.110	0.200	0.090
L7	24.7	2700	1143	270	9	0.030	0.100	0.100	0.200	0.085
L8	26.7	2580	1151	750	16	0.027	0.100	0.100	0.200	0.075
Older GLOFs										
UBK		4040	211	290	8	0.039	0.100	0.100	0.200	0.090
UDK		3340	271	130	7	0.056	0.100	0.110	0.200	0.100
Other reaches										
KJK		3360	20	35	5	0.061				0.085
N2[d]	8.2	3940	33	245	10	0.115	na	na	na	0.150
KK		2840	44	45	6	0.052				0.105
TK		3590	45	70	7	0.080				0.115
L3[d]	9.4	3790	221	335	6	0.056	na	na	na	0.100
IK		3340	306	115	8	0.056				0.110
L6[d]	20.7	2840	402	65	6	0.055	na	na	na	0.105
N4[d]		2840	685	55	5	0.020				0.080

[a] N = reaches along 1977 GLOF route; L = reaches along the 1985 GLOF route; UBK = Upper Bhoti Kosi; UDK = Upper Dudh Kosi; MDK = Middle Dudh Kosi; IK = Imja Khola; KJK = Kyajo Khola; KK = Kyashar Khola; TK = Thame Khola. Refer to Fig. 2 for reach locations.

[b] Determined from method described by Arcement and Schneider (1989).

[c] Determined using Jarrett's (1984) equation, $n = 0.32S^{0.38}R^{-0.16}$.

[d] Along 1977 or 1985 GLOF route, but reach not appropriate to model the GLOF using the step-backwater method.

Hydrologic Engineering Center, 1995). The peak discharges of the GLOFs were estimated to have lasted at least 1 hr; and because the length of the reaches modeled were between 270 and 1600 m, the relatively steady flow assumption was probably satisfied (Table 1). Cross-sections were selected along a given reach so that the gradually varied flow assumption was satisfied (Figs. 6 and 7). Flow at a given cross-section was probably not one dimensional for the GLOFs or SHFFs; however, one-dimensional flow was assumed and was probably the dominant flow direction, satisfying this assumption in the step-backwater model. Seventeen of the eighteen reaches modeled had reach-averaged slopes less than 10%. Although the energy slope is probably not uniform across a cross-section or between successive cross-sections in these high-gradient channels, the deviations are assumed to be small.

3.4.2. Selecting energy-loss coefficients

Selecting appropriate channel and flood plain roughness coefficients (Manning's n) and channel expansion/contraction coefficients are important components to accurately modeling flow conditions along a surveyed reach using the step-backwater method. For extreme floods, such as the 1977 and 1985 GLOFs, considerable energy losses because of turbulence and sediment transport must be taken into account using Manning's n to estimate total energy losses (Trieste and Jarrett, 1987). If the above-men-

tioned factors are not considered when selecting Manning's *n*, total energy losses are typically underestimated, which in turn causes flood discharges to be overestimated because flow is incorrectly modeled as supercritical (Trieste and Jarrett, 1987). As pointed out by Jarrett (1984, 1987), Trieste (1992) and Trieste and Jarrett (1987), flow is primarily subcritical in natural channels for extreme floods; and supercritical flow only occurs locally with limited spatial extent. Trieste and Jarrett (1987) recommended that if flow is computed as being supercritical along a modeled reach, the initially selected Manning's *n* should be increased until flow is subcritical and approaching critical along the modeled reach. This adjustment of Manning's *n* accounts for other energy losses associated with an extreme flood. For the GLOFs modeled in this study, flow was assumed to be subcritical and approaching critical flow.

For the GLOFs, initial Manning's *n* values for the channel (n_c) and overbank areas (n_{ob}) were determined using the visual method described by Arcement and Schneider (1989) (Table 1). Using these initial Manning's *n* values to perform the step-backwater calculations for the GLOFs caused the assumption of subcritical flow to be violated at different segments of seven of the ten GLOF reaches modeled. For these seven reaches, the initially selected Manning's *n* values for the main channel were increased until flow conditions were subcritical or near critical for the entire modeled reach (Table 1). Manning's *n* was not adjusted from the initial selected values for overbank areas.

For the SHFFs, Manning's *n* was estimated using Jarrett's (1984) equation,

$$n = 0.32\, S_f^{0.38} R^{-0.16} \quad (2)$$

where R is hydraulic radius (m) and S_f is the energy slope. In this study, bed slope was substituted for energy slope. Jarrett's equation was developed for discharges ranging from 0.34 to 128 m^3/s, hydraulic radii ranging from 0.15 to 2.10 m, and slopes ranging from 0.002 to 0.04 (Jarrett, 1984). Although the slopes and discharges of channels in this study, in most cases, did not fall within the limits for which the equation was designed, the predicted Manning's *n* from Jarrett's equation are probably reasonable. For example, Marcus et al. (1992), in a study of high-gradient channels in Alaska in which several channels were not within the data limits of Jarrett's equation, showed that Jarrett's equation only slightly overpredicted Manning's *n* and provided the best estimate of Manning's *n* when compared to visual estimates and other equations.

Energy losses resulting from channel expansion and contraction are taken into account in the step-backwater method by selecting expansion and contraction coefficients. Reaches were selected and cross-sections placed so that the assumption of gradually varied flow between cross-sections was satisfied for the most part (Figs. 6 and 7). Contraction and expansion coefficient values were assigned 0.1 and 0.3, respectively, as recommended by the Hydrologic Engineering Center (1995) for gradual flow transitions.

Sensitivity analyses were performed on the selected flow-resistance and energy-loss coefficients to assess how variations in the selected values affect the water-surface profiles and estimated peak discharges. To assess the influence of the selected energy-loss coefficients on the calculated discharges, the following sensitivity analyses were performed: (i) the Manning's *n* values selected using the methods described above were varied by 10% and 25%, (ii) Manning's *n* values for the overbank areas were changed to the same value as the main channel Manning's *n*, and (iii) contraction and expansion coefficients were changed from 0.1 and 0.3 to 0 and 0.5, 0 and 0, and 0.3 and 0.7, respectively.

4. Step-backwater modeling results

4.1. 1977 Glacial-lake outburst flood

4.1.1. Reach N1

Reach N1 is located 8.6 km downstream from the breached moraine (Fig. 2). The physical characteristics of the reach are summarized in Table 1. The GLOF caused considerable erosion and deposition along this segment of the valley (Figs. 4a and 6A). The starting water-surface elevation was determined using the normal-depth method. The initially selected main channel Manning's *n* was increased 60% to obtain subcritical flow for the outburst flood (Table

1). The reconstructed water-surface profile through reach N1 for the discharge of 1900 m^3/s was reasonably well constrained at each of the eight surveyed cross-sections by the bar deposit and nonflooded surface PSIs (Fig. 9A). The computed critical-depth profile closely matches the boulder PSIs along reach N1 (Fig. 9A), suggesting that modeling flow as critical may have been a better assessment of hydraulic conditions at reach N1. Table 2 summarizes the reach-averaged hydraulics of the modeled GLOF.

4.1.2. Reach N3

Reach N3 is located 11.5 km downstream from the breached moraine (Fig. 2). Erosion and deposition by the GLOF was minimal along this reach because the bedrock and coarse-grained colluvium valley boundaries resisted erosion for the most part and because the steep, narrow valley produced hydraulic conditions that transported most of the GLOF sediment through the reach (Figs. 4b and 6B). Immediately downstream from XS2, the valley narrows and steepens (Fig. 6B), providing a critical-depth control for the starting water-surface elevation of the GLOF. Undisturbed, pre-1977-age vegetation and poorly developed soil along the left margin of the bedrock ledge at XS2 were used to delineate the maximum stage of the GLOF (Fig. 9B). Using the critical-depth method and the maximum stage PSI at XS2, the GLOF discharge was estimated at 1500 m^3/s. Upstream from the critical-depth control, the initially selected main channel Manning's n value was increased 40% so that flow was subcritical for the modeled reach (Table 1). The reconstructed water-surface profile upstream from the critical-depth control was constrained by deposit and nonflooded surface PSIs at five of the nine cross-sections (Fig. 9B). Table 2 summarizes the reach-averaged hydraulics of the modeled GLOF.

4.2. Glacial-lake outburst flood

4.2.1. Reach L2

Reach L2 is located 7 km downstream from the breached moraine (Fig. 2). Reach boundary conditions and geomorphic features produced by the GLOF are illustrated in Figs. 5a and 7A. At the furthest downstream cross-section, the valley steepens abruptly providing a critical-depth control (Fig. 7A). A small deposit of pebbles and cobbles just below a nonflooded surface at XS10 were used to delineate the maximum stage of the GLOF. Using the critical-depth method and the PSIs at XS10, the GLOF discharge was estimated at 2350 m^3/s (Fig. 10A). Upstream from the critical-depth control, the initially selected main channel Manning's n was increased 25% so that the modeled flow was subcritical (Table 1). Using this approach, the reconstructed water-surface profile upstream from the critical-depth control section was constrained by the nonflooded PSIs, but was at least 1 m higher than the deposit PSIs

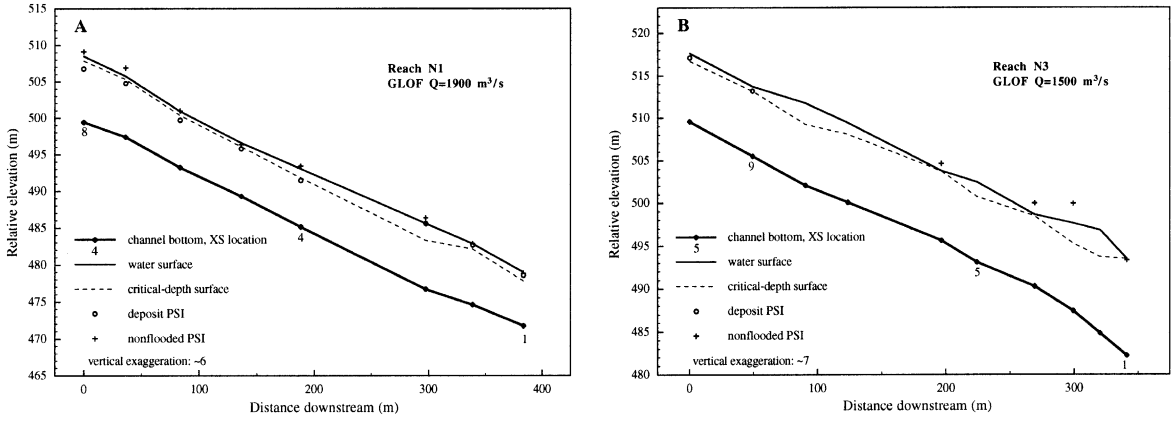

Fig. 9. Computed water-surface profile and comparison with PSIs for the 1977 GLOF at reach N1 (A) and at reach N3 (B).

Table 2
Summary of reach-averaged and ranges of (in parentheses below the reach average) hydraulic variables of the modeled GLOF reaches

Study reach[a]	Total discharge (m^3/s)	Channel discharge (m^3/s)	Energy slope	Total velocity (m/s)	Channel velocity (m)	Total flow width (m)	Channel flow width (m)	Total hydraulic radius (m)	Channel hydraulic radius (m)	Total Froude number	Channel Froude number
N1	1900	1624	0.071	3.98	5.30	121	49	3.70	5.79	0.64	0.68
		(1401–1856)	(0.045–0.089)	(3.28–4.48)	(4.72–5.73)	(109–133)	(40–60)	(3.41–4.26)	(5.13–6.71)	(0.49–0.74)	(0.56–0.75)
N3	1500	1456	0.071	5.85	6.26	44	32	4.93	6.37	0.74	0.77
		(1381–1491)	(0.032–0.118)	(4.53–7.57)	(4.77–8.25)	(34–61)	(19–39)	(4.02–5.89)	(5.61–7.83)	(0.52–0.94)	(0.54–1.00)
L2	2350	1863	0.049	4.24	6.07	122	45	4.75	6.50	0.60	0.73
		(1371–2337)	(0.033–0.093)	(2.94–8.29)	(5.17–8.65)	(46–180)	(28–62)	(3.42–5.56)	(5.68–7.46)	(0.40–1.00)	(0.62–0.97)
L1	2250	1914	0.060	4.42	5.92	113	49	4.58	6.36	0.63	0.72
		(1615–2249)	(0.029–0.125)	(3.27–7.91)	(4.33–7.96)	(45–222)	(29–103)	(2.99–5.75)	(4.28–7.84)	(0.53–1.00)	(0.51–1.00)
L4	2275	1608	0.072	4.07	5.62	146	40	4.43	6.61	0.58	0.66
		(986–2252)	(0.054–0.118)	(2.49–8.20)	(3.90–8.55)	(41–264)	(25–56)	(3.33–5.40)	(4.97–7.93)	(0.41–1.00)	(0.52–0.98)
L5	1725	1593	0.0330	4.68	5.41	68	43	4.88	6.47	0.63	0.65
		(1299–1725)	(0.008–0.055)	(3.12–5.94)	(3.71–6.85)	(54–80)	(25–57)	(3.64–7.18)	(4.98–9.36)	(0.38–0.83)	(0.35–0.94)
L7	1575	1499	0.031	4.87	5.53	67	44	4.37	5.73	0.70	0.70
		(1370–1535)	(0.018–0.047)	(3.58–6.11)	(4.51–6.62)	(50–82)	(37–52)	(3.65–5.07)	(5.15–6.22)	(0.49–0.88)	(0.56–0.88)
L8	1375	1302	0.029	4.57	4.98	66	47	4.16	5.19	0.66	0.66
		(1063–1375)	(0.014–0.057)	(3.41–5.76)	(3.69–6.56)	(41–97)	(32–61)	(3.18–5.07)	(4.28–6.14)	(0.48–0.83)	(0.48–0.89)
UBK	400	342	0.036	2.93	3.72	64	30	2.04	2.95	0.64	0.67
		(261–385)	(0.011–0.054)	(2.07–3.81)	(2.60–4.27)	(46–77)	(18–36)	(1.63–2.57)	(2.39–3.83)	(0.42–0.87)	(0.42–0.89)
UDK	700	670	0.056	4.22	4.48	59	42	2.52	3.13	0.76	0.80
		(638–684)	(0.035–0.084)	(3.31–5.21)	(3.78–5.27)	(46–77)	(26–50)	(2.05–2.83)	(2.71–4.24)	(0.59–0.93)	(0.60–0.99)

Total refers to the entire cross sections modeled and includes the main channel and overbank areas.
Channel refers to the main channel of flow.

[a] N refers to reaches modeled along the 1977 GLOF route, L refers to reaches modeled along the 1985 GLOF route, UBK and UDK are older GLOF reaches modeled on the upper Bhoti Kosi and upper Dudh Kosi.

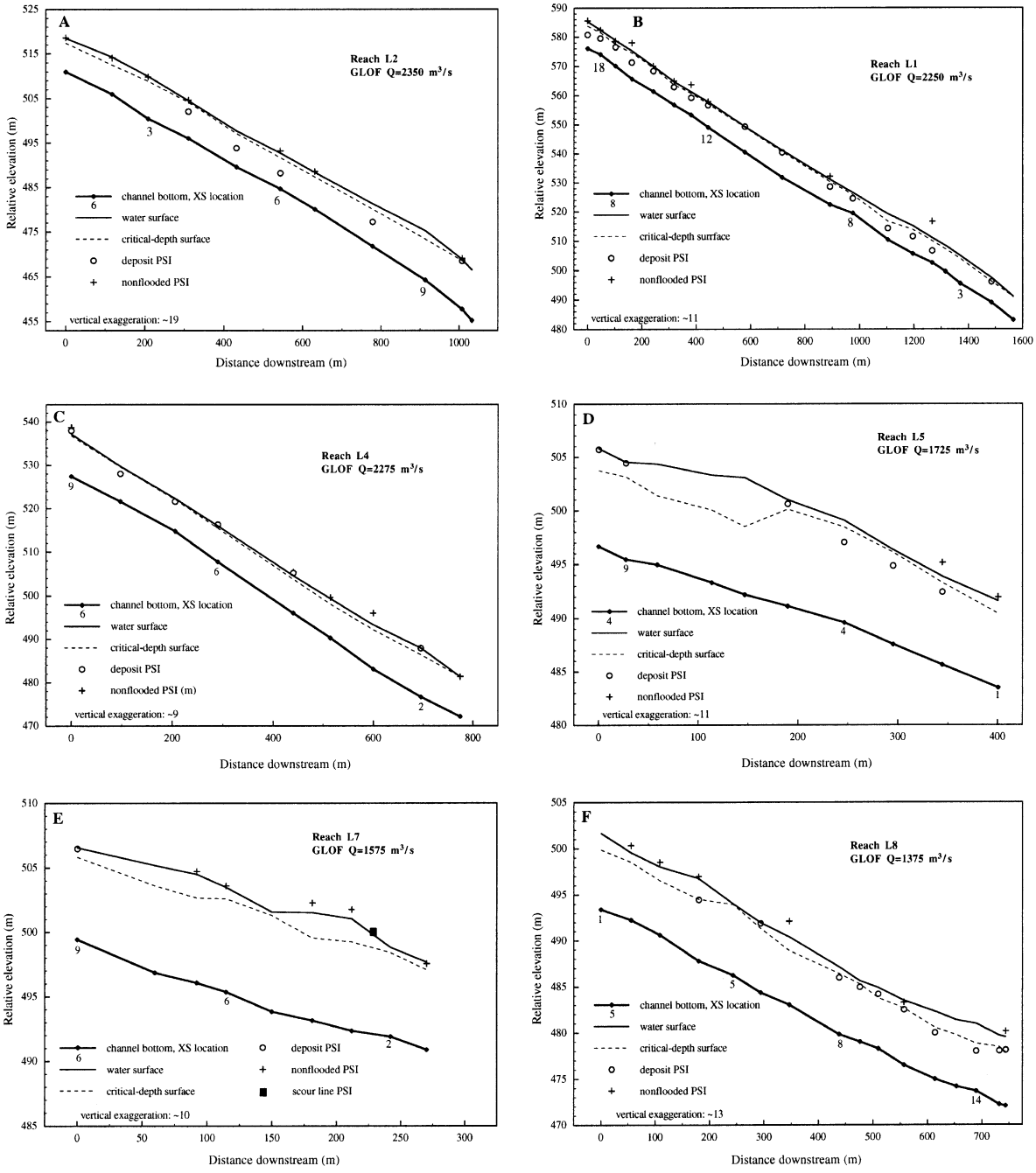

Fig. 10. Computed water-surface profile and comparison with PSIs for the 1985 GLOF at reach L2 (A), reach L1 (B), reach L4 (C), reach L5 (D), reach L7 (E), and reach L8 (F).

(Fig. 10A). This indicates some uncertainty in the water-surface elevation upstream from the critical-depth control. Table 2 summarizes the reach-averaged hydraulics of the modeled GLOF.

4.2.2. Reach L1

Reach L1 is located approximately 11 km downstream from the breached moraine (Fig. 2). Reach boundary conditions and geomorphic features produced by the GLOF are illustrated in Figs. 5b and 7B. At XS1, the valley narrows and steepens (Fig. 7B), providing critical-depth control for the starting water-surface elevation. Upstream from XS1, the crest of a longitudinal bar at XS2 was used to delineate the stage of the GLOF. Using the critical-depth method combined and the PSI at XS2, the estimated GLOF discharge was 2250 m^3/s. Upstream from the critical-depth control section, the initially selected main channel Manning's n value was increased 40% (Table 1) so that the modeled flow was subcritical. For the estimated discharge of 2250 m^3/s, the reconstructed water-surface profile corresponded fairly well with the deposit and nonflooded surface PSIs (Figs. 7B and 10B). Table 2 summarizes the reach-averaged hydraulics of the modeled GLOF.

4.2.3. Reach L4

Reach L4 is located approximately 15.5 km downstream from the breached moraine (Fig. 2). Reach boundary conditions and geomorphic features produced by the GLOF are illustrated in Figs. 1b and 7C. The narrow valley between XS2 and XS1 provided a critical-depth control for the starting water-surface elevation. A nonflooded surface at XS1, combined with a thin veneer of cobbles and boulders overlying a lower glaciofluvial terrace at XS2, were used to delineate the maximum stage of the GLOF (Fig. 7C). Using the critical-depth method in conjunction with the PSIs at XS1 and XS2, the estimated GLOF discharge was 2275 m^3/s (Fig. 10C). Upstream from the critical-depth control, the initially selected main channel Manning's n value was increased 40% so that the modeled flow was subcritical. Upstream from the critical-depth control to XS4, the reconstructed water-surface profile corresponded reasonably well with the PSIs (Fig. 10C). Upstream from XS4, the computed water-surface profile was 0.68 to 0.77 m lower than the highest deposit PSIs at XS9 and XS5, respectfully (Fig. 10C). The poor match between the water-surface profile and PSIs upstream from XS4 is partly attributed to modeling flow through this expanding segment of the reach (Fig. 7C). Table 2 summarizes the reach-averaged hydraulics of the modeled GLOF.

4.2.4. Reach L5

Reach L5 is located approximately 22 km downstream from the breached moraine (Fig. 2). Reach boundary conditions and geomorphic features produced by the GLOF are illustrated in Figs. 5c and 7D. The starting water-surface elevation was determined using the normal-depth method. The initially selected main channel Manning's n was increased 10% so that the modeled flow was subcritical (Table 1). Through reach L5, the reconstructed water-surface profile, at a discharge of 1725 m^3/s, was fairly well constrained by the deposit and nonflooded surface PSIs with the best matches occurring at XS6, XS9, and XS10 (Fig. 10D). Table 2 summarizes the reach-averaged hydraulics of the modeled GLOF.

4.2.5. Reach L7

Reach L7 is located on the Dudh Kosi, approximately 24.7 km downstream from the breached moraine (Fig. 2). Reach boundary conditions and geomorphic features produced by the GLOF are illustrated in Fig. 7E. Nonflooded surfaces were the primary PSIs identified along reach L7. Deposit PSIs at high elevations were lacking along reach L7 with the exception of XS9. A distinct scour line on a large boulder (greater than 15 m in diameter) with etchings was identified between XS2 and XS3. The starting water-surface elevation at XS1 was determined using the normal-depth method. The main channel Manning's n did not have to be increased from its initially selected value of 0.10 to attain subcritical flow for the GLOF using the step-backwater method. The reconstructed water-surface profile through reach L7 was fairly well constrained by the PSIs (Fig. 10E) and was associated with a discharge of 1575 m^3/s. Table 2 summarizes the reach-averaged hydraulics of the modeled GLOF.

4.2.6. Reach L8

Reach L8 is located on the Dudh Kosi, approximately 26.7 km downstream from the breached moraine (Fig. 2). Reach boundary conditions and geomorphic features produced by the GLOF are illustrated in Fig. 7F. The starting water-surface

elevation was determined using the normal-depth method. The main channel Manning's *n* did not have to be increased from its initially selected value of 0.10 to attain subcritical flow for the GLOF using the step-backwater method. The reconstructed water-surface profile through reach L8 adequately matched the longitudinal bar deposit and nonflooded surface PSIs and was associated with a discharge of 1375 m^3/s (Fig. 10F). The computed critical-depth profile more closely matched the deposit PSIs along reach L8 (Fig. 10F), suggesting that modeling flow as critical may have been a better assessment of hydraulic conditions at reach L8. Table 2 summarizes the selected reach-averaged hydraulic parameters of the modeled GLOF through reach L8.

4.3. Older outburst floods

4.3.1. Upper Bhoti Kosi, UBK

The upper Bhoti Kosi reach is located in the upper Bhoti Kosi drainage (Fig. 2) at an elevation of 4040 m. Reach boundary conditions and geomorphic features produced by the GLOF are illustrated in Fig. 8a. The starting water-surface elevation at the furthest downstream cross-section was determined using the normal-depth method. The main channel Manning's *n* was not increased from its initially selected value of 0.10 to attain subcritical flow for the GLOF using the step-backwater method. The reconstructed water-surface profile through the upper Bhoti Kosi reach matched the cobble-boulder deposit PSIs fairly well (Fig. 11A) and was associated with a discharge of 400 m^3/s. Table 2 summarizes the selected reach-averaged hydraulic parameters of the modeled older GLOF through reach UBK.

4.3.2. Upper Dudh Kosi, UDK

The upper Dudh Kosi reach is located in the upper Dudh Kosi drainage basin (Fig. 2) at an elevation of 3340 m. Reach boundary conditions and geomorphic features produced by the GLOF are illustrated in Fig. 8b. The starting water-surface elevation at the furthest downstream cross-section was determined using the normal-depth method. The main channel Manning's *n* was increased 10% to attain subcritical flow for the GLOF. The main channel Froude numbers ranged from 0.59 to 0.93 with a reach-averaged main channel Froude number of 0.76. Through the upper Dudh Kosi reach, the reconstructed water-surface profile at a discharge of 700 m^3/s was fairly well constrained by the deposit PSIs (Fig. 11B). Table 2 summarizes the selected reach-averaged hydraulic parameters of the modeled older GLOF through reach UDK.

4.4. Seasonal high flow floods

The peak discharges of SHFFs were estimated at the ten GLOF reaches modeled and at eight additional reaches. These reaches are located in several different streams at varying elevations with various drainage areas (Table 1; Fig. 2). The reaches range in length from 35 to 1565 m, have channel widths ranging from 10 to 30 m, and have average gradients

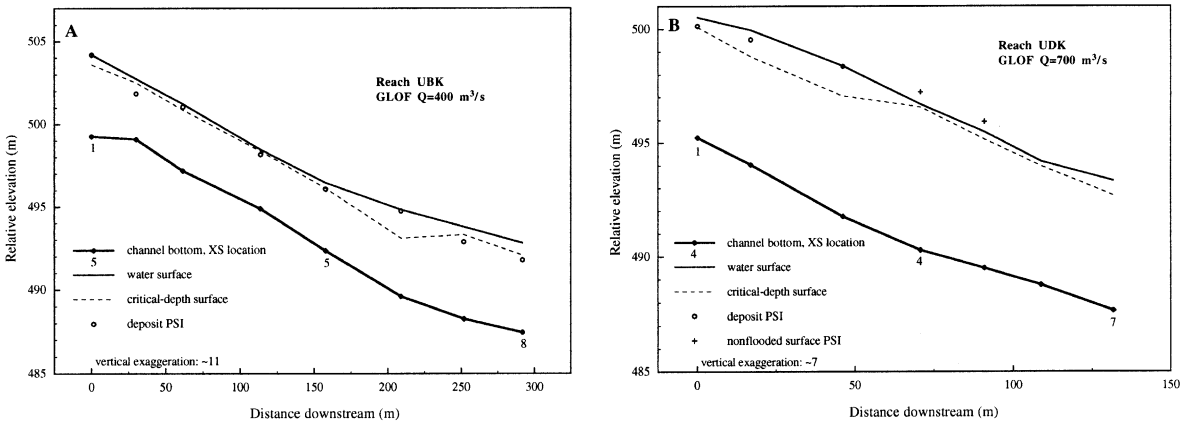

Fig. 11. Computed water-surface profile and comparison with PSIs for the older GLOFs at reach UBK (A) and at reach UDK (B).

ranging from 0.020 to 0.115 (Table 1). The modeled reaches can generally be classified as riffles with channel beds of cobbles-boulders and/or bedrock with isolated cobbles and boulders. Distinct white-

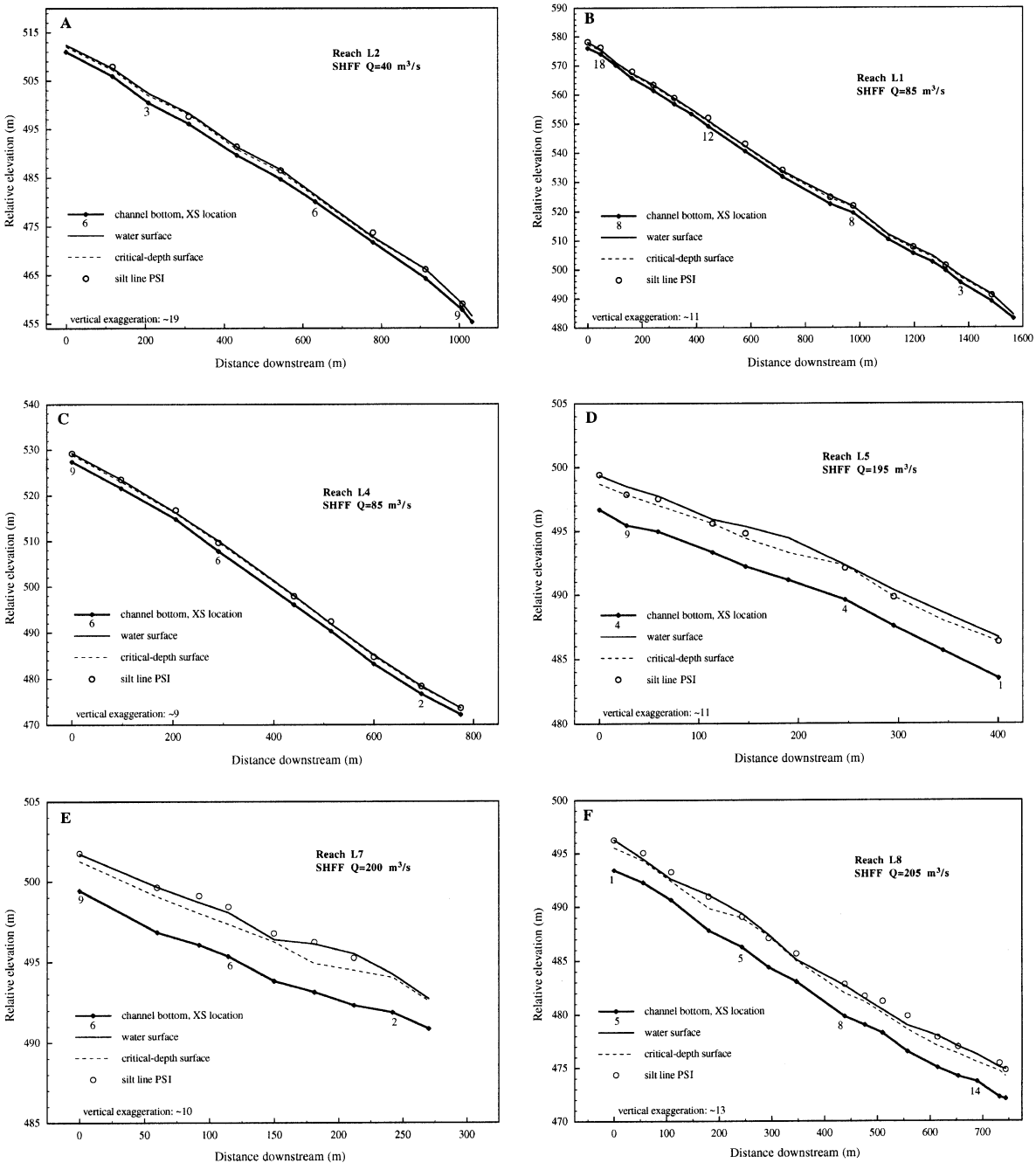

Fig. 12. Computed water-surface profile and comparison with PSIs for the SHFFs at the 1977 GLOF study reaches (A–D), 1985 GLOF study reaches (E–L), older GLOF reaches (M and N), and tributary reaches (O–R).

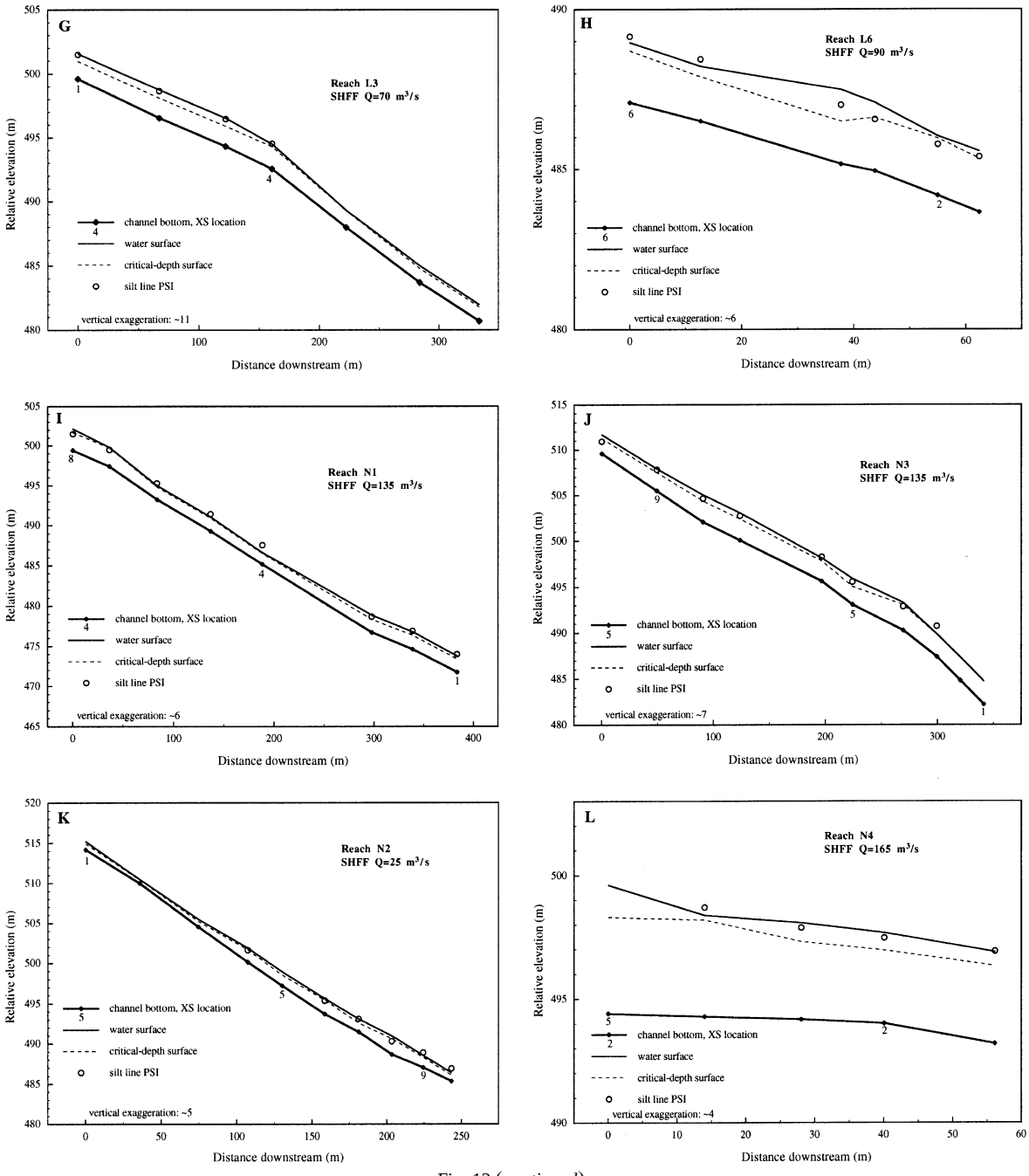

Fig. 12 (*continued*).

gray silt lines along the channel margins were used to delineate the peak stage of the SHFF. The study reaches IK, KK, TK, N3, L2, L1, and L4 are located immediately upstream from distinct stable steps, allowing the critical-depth method to be used to determine the starting water-surface elevation and SHFF

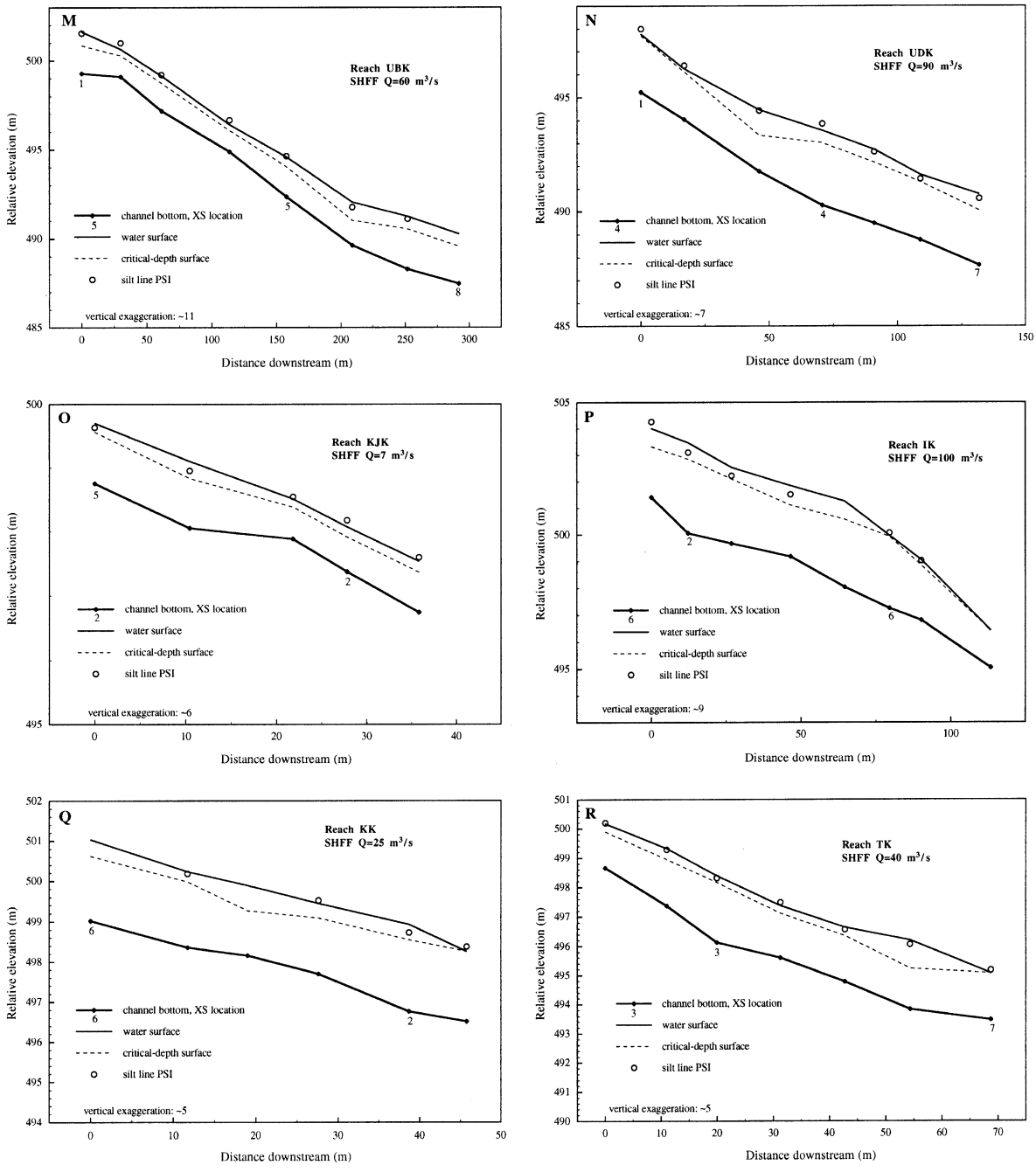

Fig. 12 (*continued*).

discharge in conjunction with geologic evidence. At the study reaches KYK, N2, N1, N4, L3, L6, L5, L7, and L8, the initial starting water-surface elevation was determined using the normal-depth method. All reaches were modeled as subcritical flow, and averaged reach Froude numbers ranged from 0.66 to

0.82. As illustrated in Fig. 12, the computed water-surface profiles are in close agreement with the PSIs that delineate SHFFs along the 18 reaches. For the 18 reaches modeled, the SHFFs estimated peak discharges ranging between 7 and 205 m^3/s, reach-averaged velocities ranging from 1.68 to 4.25 m/s, reach-averaged hydraulic radiuses ranging from 0.41 to 2.16 m, and reach-averaged flow widths ranging from 10.02 to 31.97 m (Table 3).

4.5. Quality of step-backwater modeling

4.5.1. Glacial-lake outburst floods

The uncertainty of the GLOF discharge estimates based on "best match" water-surface profiles ranged from −42% to 36% (Table 4). These uncertainty discharge estimates were determined by reconstructing the water-surface profile along each modeled reach so that (i) the deposit PSIs were above the water-surface profile (conservative, lower discharge estimate) and (ii) the nonflooded surface PSIs were below the water-surface profile (liberal, upper discharge estimate). Although the "best match" discharge estimate provided the most reasonable discharge estimate because it utilized both deposit and nonflooded surface PSIs, the lower and upper discharge estimates provided a potential range of discharge estimates based on the geomorphic evidence.

The most reliable GLOF discharge estimates, based on reach selection and the best matches between the computed water-surface profiles and geomorphic evidence, were obtained at reaches N1, N3, L2, L1, and L4 (Figs. 9A, B, 10A, B and C, respectively). Of these five reaches, four reaches (N3, L2, L1, and L4) were just upstream from constrictions where there was critical-depth control and geomorphic evidence to define the maximum stage of the GLOFs (Figs. 6B, 7A, B and C, respectively). As pointed out by Jarrett (1987), the critical-depth method for estimating discharge in high-gradient streams is preferred because the estimated discharge is independent of Manning's *n*. When the discharge estimate calculated from the critical-depth method at the critical-depth control was applied to the remainder of those reaches, the water-surface profiles at reaches N3, L2, L1, and L4 were in reasonably close agreement with the PSIs at their respective reaches (Figs. 9B, 10A, B and C, respectively). Note that upstream from the critical-depth control at reaches N3, L2, L1, and L4, flow was modeled as subcritical, but approaching critical-flow conditions.

Although the step-backwater calculations may be accurate for the 1985 GLOF at reaches L5, L7, and L8, the discharge estimates are sensitive to the selected energy-loss coefficients, principally Manning's *n*. Recall that Manning's *n* was used not only to account for energy losses associated with grain roughness, but also used to account for additional energy losses from turbulence, erosion, and sediment transport that occurred during the GLOFs. Because there is uncertainty in assigning energy-loss coefficients, underestimating or overestimating the energy-loss coefficients in the model can result in inaccurate discharge estimates. Additionally, at these reaches, either fewer PSIs clearly define the maximum stage of the GLOF or PSIs are not in complete agreement with each other (Fig. 10D, E and F). Although the match between the water-surface profile and PSIs is acceptable, subtle inconsistencies between the water-surface profile and PSIs suggest the actual flow conditions were not being completely and accurately modeled.

For the older GLOF reaches there is a reasonable match between the PSIs and computed water-surface profiles (Fig. 11A and B); however, there is uncertainty as to whether the channel geometry had been modified since the older GLOFs occurred at the upper Bhoti Kosi and upper Dudh Kosi reaches. Thus, the older GLOF discharge estimates are based on the present channel/valley geometry and not necessarily the channel/valley geometry during peak flow conditions of the older GLOFs. Another source of uncertainty is that both the upper Bhoti Kosi reach and upper Dudh Kosi reach gradually expand in the downstream direction. This gradual expansion introduces error in the computed water-surface profile because flow is diverging.

4.5.2. Seasonal high flow floods

The step-backwater modeling of the SHFFs at the various reaches seems to accurately represent those flows. At the older GLOF and tributary reaches, the silt-clay PSIs delineate the largest SHFF that has occurred at those reaches. The abundant seasonal high flow flood PSIs at the reaches modeled were

Table 3
Summary of reach-averaged and ranges of (in parentheses below the reach average) hydraulic variables of the modeled SHFF reaches

Study reach[a]	Drainage area (km^2)	Reach elevation (m)	Discharge (m^3/s)	Energyslope	Velocity (m/s)	Flow width (m)	Hydraulic radius (m)	Froude number
KJK	20	3360	7	0.071	1.68	10.02	0.41	0.82
				(0.040–0.105)	(1.44–2.08)	(7.60–13.65)	(0.33–0.53)	(0.65–1.00)
N2	33	3940	25	0.119	1.84	17.49	0.74	0.66
				(0.085–0.201)	(1.64–2.05)	(13.31–27.81)	(0.48–0.90)	(0.56–0.83)
L2	41	4080	40	0.063	2.25	18.77	0.94	0.71
				(0.037–0.120)	(1.73–3.37)	(10.13–30.89)	(0.69–1.26)	(0.57–1.00)
KK	44	2840	25	0.073	1.98	15.16	0.74	0.69
				(0.041–0.157)	(1.55–2.31)	(9.24–19.70)	(0.48–0.89)	(0.54–1.00)
TK	45	3590	35	0.082	2.32	14.32	0.97	0.71
				(0.030–0.155)	(176–2.91)	(10.81–20.08)	(0.78–1.26)	(0.44–1.00)
UBK	211	4040	60	0.033	2.17	21.52	1.19	0.60
				(0.008–0.054)	(1.29–2.51)	(15.16–29.85)	(0.88–1.51)	(0.33–0.78)
L3	221	3790	70	0.057	2.69	19.52	1.24	0.74
				(0.035–0.97)	(2.23–3.36)	(16.53–26.33)	(1.08–1.50)	(0.60–0.96)
UDK	271	3340	90	0.054	2.68	24.07	1.37	0.70
				(0.018–0.090)	(1.97–3.35)	(14.31–41.65)	(0.86–1.93)	(0.44–0.89)
L1	295	3710	85	0.059	2.60	26.02	1.24	0.72
				(0.026–0.114)	(1.98–3.39)	(16.59–51.97)	(0.78–1.58)	(0.50–1.00)
IK	306	3340	100	0.068	2.74	23.94	1.33	0.72
				(0.035–0.125)	(1.93–3.64)	(15.86–31.03)	(1.08–1.69)	(0.53–1.00)
N1	339	3840	135	0.073	3.11	28.91	1.45	0.80
				(0.046–0.107)	(2.46–3.61)	(20.89–42.09)	(1.21–1.83)	(0.60–0.90)
L4	356	3440	85	0.080	3.08	19.39	1.33	0.82
				(0.060–0.119)	(2.57–3.62)	(6.15–25.99)	(1.19–1.52)	(0.72–1.00)
N3	365	3790	135	0.091	3.51	20.76	1.70	0.80
				(0.042–0.142)	(2.68–4.69)	(12.76–31.10)	(1.49–1.99)	(0.58–1.00)
L6	402	2840	90	0.058	2.95	18.27	1.55	0.73
				(0.018–0.096)	(1.96–3.72)	(15.11–21.58)	(1.37–1.90)	(0.43–0.94)
N4	685	2840	165	0.040	4.25	12.39	2.16	0.76
				(0.025–0.062)	(3.65–5.11)	(10.44–13.36)	(1.99–2.28)	(0.62–0.93)
L5	1093	2770	195	0.034	3.10	31.97	1.94	0.68
				(0.014–0.068)	(1.98–4.61)	(19.17–48.91)	(1.45–2.61)	(0.44–0.99)
L7	1143	2700	200	0.035	3.31	28.46	2.02	0.73
				(0.013–0.059)	(2.34–4.19)	(22.27–33.34)	(1.52–2.37)	(0.46–0.94)
L8	1151	2580	205	0.029	3.34	31.82	1.87	0.75
				(0.011–0.047)	(2.45–4.20)	(17.78–49.00)	(1.38–2.50)	(0.49–0.95)

[a]N refers to reaches modeled along the 1977 GLOF route, L refers to reaches modeled along the 1985 GLOF route, UBK = upper Bhoti Kosi, UDK = upper Dudh Kosi, IK = Imja Khola, TK = Thame Khola, KJK = Kyajo Khola, KK = Kyashar Khola.

Table 4
Summary of best match discharges and bracketing discharges for the 1977, 1985, and older glacial-lake outburst floods

Study reach[a]	Best match peak discharge estimate (m^3/s)	Lower bracketing peak discharge estimate for deposit PSI (m^3/s)	Percent change in peak discharge estimate	Upper bracketing peak discharge estimate for deposit PSI (m^3/s)	Percent change in peak discharge estimate	Lower bracketing peak discharge estimate for nonflooded PSI (m^3/s)	Percent change in peak discharge estimate	Upper bracketing peak discharge estimate for nonflooded PSI (m^3/s)	Percent change in peak discharge estimate
N1	1900	1200	−37	1900	0	1900	0	2400	26
N3	1500	1300	−13	1500	0	1500	0	2000	33
L2	2350	2200	−6	2350	0	2350	0	2700	15
L1	2250	1300	−42	2250	0	2250	0	3100	38
L4	2275	1500	−34	2900	28	2275	0	2800	23
L5	1725	1100	−36	1725	0	1725	0	2350	36
L7	1575	1575	0	1575	0	1575	0	1850	17
L8	1375	900	−35	1375	0	1375	0	1700	24
UBK	400	250	−38	400	0	na	na	na	na
UDK	700	600	−14	700	0	875	25	875	25

[a] N refers to reaches modeled along the 1977 GLOF route, L refers to reaches modeled along the 1985 GLOF route, UBK = upper Bhoti Kosi, and UDK = upper Dudh Kosi.

usually in close agreement with the computed water-surface profile. The uncertainty of the SHFF discharge estimates based on "best match" water-surface profile ranged from −43% to 43% (Table 5). These uncertainty discharge estimates were determined by reconstructing the water-surface profile along each modeled reach so that silt-clay PSIs were above the water-surface profile (conservative, lower discharge estimate) and below the water-surface profile (liberal, upper discharge estimate).

Although the use of Jarrett's (1984) equation (Eq. (2)) to estimate Manning's *n* for the channels studied is debatable because many of the slopes and discharges fell outside of the data range used to develop the equation, the SHFFs modeled were usually close to critical flow using the Manning's *n* value calculated from Jarrett's equation. It has been suggested that in high-gradient, mountainous channels, flow is usually close to critical (Jarrett, 1984; Trieste, 1992; Trieste and Jarrett, 1987; Tinkler, 1996; Grant, 1997). For most of the SHFFs modeled in this study, flows were close to critical, which suggests that the Manning's *n* calculated using Jarrett's equation reasonably estimated the channel roughness of streams in the study area (Fig. 12, Table 3).

Perhaps the greatest uncertainty in modeling the SHFFs is the channel geometry. Although the flows during the field season were low, they were high enough to prevent channel crossing and surveying the topography within the channel. To compensate for the lack of surveying information within the channel, for each modeled reach the channel was assumed to be (i) rectangular between the left and right bank water's edge at the time of measurement and (ii) at least 1 m lower than the water-surface elevation at the time of measurement based on visual estimates and probing. For the latter assumption, the channel-bottom elevation was additionally lowered by the elevation difference between the SHFF PSI and the water surface at the time of measurement. This elevation adjustment to the channel bottom was necessary because the elevation difference between the SHFF PSI and water surface at the time of

Table 5
Summary of best match discharges and bracketing discharges for the seasonal high flow floods

Study reach[a]	Best match peak discharge estimate (m^3/s)	Lower bracketing peak discharge estimate for deposit PSI (m^3/s)	Percent change in peak discharge estimate	Upper bracketing peak discharge estimate for deposit PSI (m^3/s)	Percent change in peak discharge estimate
N1	135	110	−19	170	26
N3	135	105	−22	165	22
L2	40	35	−13	50	25
L1	85	65	−24	110	29
L4	85	60	−29	110	29
L5	195	150	−23	205	5
L7	200	180	−10	235	18
L8	205	180	−12	260	27
UBK	60	50	−17	80	33
UDK	90	65	−28	120	33
KJK	7	4	−43	10	43
N2	25	20	−20	30	20
KK	25	20	−20	30	20
TK	35	30	−14	40	14
L3	70	65	−7	75	7
IK	100	80	−20	115	15
L6	90	65	−28	105	17
N4	165	150	−9	190	15

[a] N refers to reaches modeled along the 1977 GLOF route, L refers to reaches modeled along the 1985 GLOF route, UBK = upper Bhoti Kosi, UDK = upper Dudh Kosi, IK = Imja Khola, TK = Thame Khola, KJK = Kyajo Khola, KK = Kyashar Khola.

measurement increased with increasing drainage area. This surveying adjustment was consistently applied to each modeled reach in an effort to minimize error or at least be consistent on the amount of error introduced. Because of the lack of channel bottom surveying information, the discharges of the SHFFs may be underestimated or overestimated. Precise characterization of the channel bottom probably had minimal effects on the estimated GLOF discharges because of the greater flow depths associated with the GLOFs.

4.5.3. Sensitivity analysis on the selection of friction- and energy-loss coefficients

To assess the influence or sensitivity of the selected Manning's *n* values and the contraction/expansion coefficient values on the step-backwater method, these values were varied. Varying contraction and expansion coefficient values of 0 and 0.5, 0 and 0, and 0.3 and 0.7, respectively, while keeping Manning's *n* values constant had little effect on the computed step-backwater water-surface profile. For example, using conservative contraction and expansion coefficient values of 0.3 and 0.7, respectively, for abrupt flow transitions, discharge did not change or decreased by only 4.35%. These results suggest that the energy losses associated with contraction and expansion have a minimal effect on the estimated discharges, regardless of the values selected.

Varying Manning's *n* for the main channel had the greatest influence on the estimated discharges. Increasing the main channel Manning's *n* by 10% caused the estimated discharge to decrease by 5.5% to 9.1% for the GLOFs and decrease by 5.9% to 10.0% for the SHFFs. Increasing the main channel Manning's *n* by 25% caused the estimated discharge to decrease by 13.7% to 20.0% for the GLOFs and 14.3% to 20.7% for the SHFFs. The changes in the SHFF discharges that occurred in response to the changes in Manning's *n* are similar in magnitude to the Manning's *n* changes documented by Wohl (1998) in a study of high-gradient channels. The results in this study show that the estimated discharge values are influenced by the selection of the main channel Manning's *n*. With the exception of reach L2, reducing the *n* values predicted by Jarrett's (1984) equation (Eq. (2)) by 10% caused sections of the modeled SHFF not to be subcritical.

Adjusting the overbank Manning's *n* by −10%, −25%, 10%, and 25%, while keeping the main channel constant had a minimal effect on the estimated GLOF discharges. For example, increasing overbank Manning's *n* by 25% either did not change the discharge or decreased the discharge estimate by only 4.2%. Similarly, decreasing overbank Manning's *n* by 25%, either did not change the discharge or increased the total discharge estimate by only 6.3%. These results indicate that the selected overbank Manning's *n* only has a minimal effect on the outburst flood estimated discharge.

A uniform Manning's *n* for the main channel and overbank areas caused the estimated GLOF discharges to change; however, the magnitude and change in discharge were variable between reaches. In general, reaches with larger overbank areas (reaches L1, L2, L3, L4, and L6) had greater changes in discharge (ranging from −4.3% to 15.6%), whereas reaches with smaller overbank areas (reaches N1, N3, L5, L7, and L8) only had a minimal change in the estimated discharges (ranging from 1.7% to 10.1%).

In summary, the sensitivity analyses performed illustrate that varying contraction coefficients, expansion coefficients, and overbank Manning's *n* only had a minimal effect on the estimated discharges in this study. In contrast, varying the main channel Manning's *n* had the greatest effect on the estimated GLOF and SHFF discharges. Increasing the main channel Manning's *n* by 10% and 25% caused a similar magnitude decrease in the estimated discharge. These results indicate that of the energy losses quantified in the step-backwater model, the selection of the main channel Manning's *n* had the greatest influence or control on the estimated discharges of the GLOFs and SHFFs determined by using the step-backwater method.

5. Flood hydrology in the Mount Everest region

5.1. Seasonal high flow floods

The SHFF discharge estimates at the 18 reaches quantify for the first time the flood hydrology from seasonal climatic conditions in the Mount Everest region (Tables 3 and 5). The SHFF discharge esti-

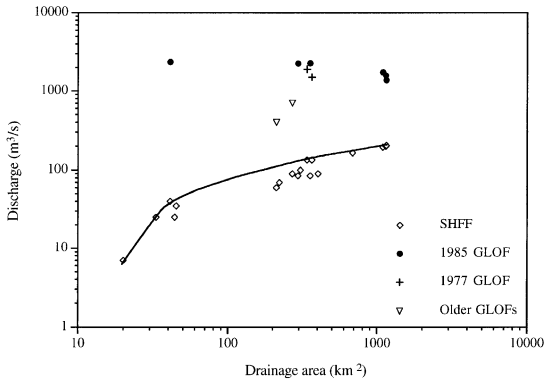

Fig. 13. Plot of the GLOF and SHFF peak discharges vs. drainage area. The solid line delineates the envelope of the maximum discharges of the SHFFs for various drainage areas.

mates only quantify the largest SHFF that has occurred at a given study site because the silt-clay PSIs only delineate the maximum SHFF. The SHFF discharge estimates provide a baseline to which the magnitude of the GLOF discharges can be compared. A plot of the SHFF discharges vs. drainage area shows that as contributing drainage area increases the discharge of the SHFFs increases (Fig. 13).

Hydrology in the study area is strongly influenced by monsoonal precipitation and late spring/early summer snowmelt and glacier runoff. Ageta (1976) and Zimmermann et al. (1986) suggested that the high mountain topography in the study area creates a rain-shadow effect that reduces the intensity and amount of monsoonal precipitation with increasing elevation. The estimated SHFF discharges in the study area show a progressive, gradual increase with increasing drainage area (Fig. 13). This trend of gradual, increasing discharges with increasing drainage area suggests that extreme flooding from intense monsoonal precipitation is unlikely in the study area because the high mountain topography impedes and minimizes the influx of intense monsoonal precipitation into the study area drainage basin.

5.2. Glacial-lake outburst floods

The estimated peak discharges of the 1977, 1985, and older GLOFs were considerably larger than the SHFFs (Fig. 13; Table 6). As drainage area increases or distance from the GLOF source increases, the difference in magnitude between the GLOFs and SHFFs decreases (Fig. 12; Table 6). At locations near the GLOF source, the discharge ratio between the GLOF and SHFF is greatest and progressively decreases downstream as the GLOF attenuates and the SHFF increases. At the reaches where the 1977 and 1985 GLOF discharges were estimated, the GLOF discharges were 7 to 60 times greater than the SHFF discharges (Fig. 13; Table 6).

Comparing the peak discharge estimates of the 1985 GLOF and SHFF along the 1985 GLOF route perhaps best illustrates changes in the peak discharges of the GLOF and SHFF with respect to distance downstream from the breached moraine and

Table 6
Summary of discharge estimates at reaches where both the GLOF and SHFF were modeled

Study reach[a]	Distance from breached moraine (km)	GLOF discharge, Q_{GLOF} (m^3/s)	SHFF discharge, Q_{SHFF} (m^3/s)	Ratio of Q_{GLOF} to Q_{SHFF}
N1	8.6	1900	135	14
N3	11.5	1500	135	11
L2	7.1	2350	40	59
L1	10.9	2250	85	27
L4	15.6	2275	85	27
L5	22.1	1725	195	9
L7	24.7	1575	200	8
L8	26.7	1375	205	7
UBK	not known	400	60	7
UDK	not known	700	90	8

[a] N refers to reaches modeled along the 1977 GLOF route, L refers to reaches modeled along the 1985 GLOF route, UBK = upper Bhoti Kosi, and UDK = upper Dudh Kosi.

increasing drainage area. For the 1985 GLOF, the peak discharge of the GLOF ranged from 2250 to 2400 m^3/s along the upper 16 km of the flood route and was 30 to 60 times greater than SHFF (Fig. 14; Table 6). The lack of a decreasing trend in the GLOF discharge along the upper 16 km of the 1985 GLOF route reflects the uncertainty in the GLOF discharge estimates for these reaches (Fig. 14; Table 6). Additionally, the direction of error associated with the GLOF discharge estimates at reaches L2, L1, and L4 influences the discharge relationship between these reaches (Table 6). At 27 km downstream from the breached moraine, the peak discharge of the 1985 GLOF attenuated to 1375 m^3/s and was seven times greater than SHFF (Fig. 14; Table 6). The downstream decline in the ratio of the 1985 GLOF peak discharge to the SHFF peak discharge is the result of the downstream attenuation of the GLOF peak discharge and the increased peak discharge of SHFF because of increased contributing drainage area and the increased effects of monsoonal precipitation at lower elevations. The most distinct changes in the discharge ratio between the GLOF and SHFF occur at major confluences: the Langmoche Khola and Bhoti Kosi confluence and the Bhoti Kosi and Dudh Kosi confluence (Fig. 14). Immediately downstream from these confluences, the peak discharge of the SHFF approximately doubled because of the considerable increase in drainage area, resulting in a sharp decrease in the discharge ratio between the GLOF discharge and SHFF discharge.

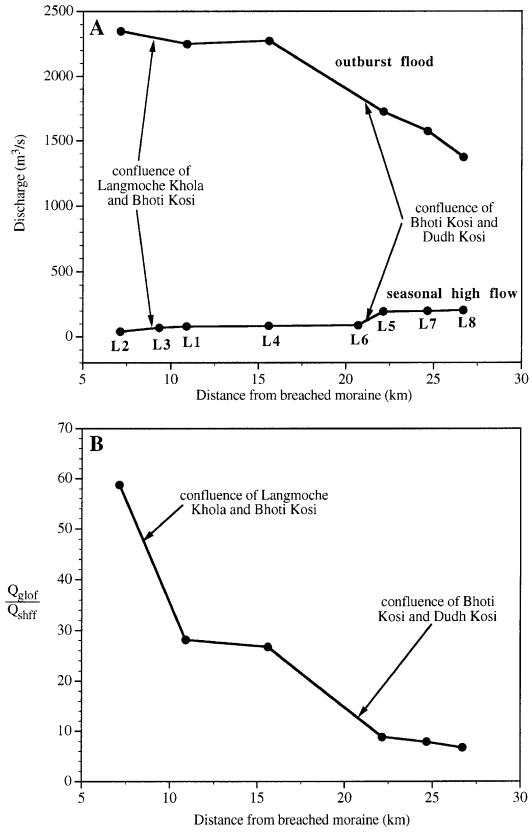

Fig. 14. (A) Peak discharges of the six GLOF study reaches and eight SHFF study reaches along the 1985 GLOF route. (B) Ratio of the GLOF peak discharge to the SHFF peak discharge at the six study reaches along the 1985 GLOF route.

The 1977 GLOF had an estimated peak discharge of 1900 m^3/s at reach N1, which is approximately 8.6 km downstream from the breached moraine. At reach N1, the peak discharge of the GLOF was about 14 times greater than the peak discharge of the SHFF at that location (Table 6). At reach N3, approximately 3 km downstream from reach N1 and 11.5 km downstream from the breached moraine, the 1977 GLOF attenuated to 1500 m^3/s and was 11 times greater than the peak discharge of the SHFF at that location (Fig. 13; Table 6). It was mentioned earlier that the peak discharge of the 1985 GLOF was larger than the 1977 GLOF because of the lack of paleoflood evidence for the 1977 GLOF downstream from the Dudh Kosi and Bhoti Kosi confluence (Fig. 2). The 1977 and 1985 GLOF discharge estimates support this assumption. At reach N3, the 1977 GLOF had a peak discharge of 1500 m^3/s, which is 9.4 km upstream from the Dudh Kosi and Bhoti Kosi confluence. The 1977 GLOF discharge at reach N3 is less than the 1985 GLOF discharge at reaches L5 and L7 (Tables 2 and 4), which are located on the Dudh Kosi downstream from the Dudh Kosi and Bhoti Kosi confluence (Fig. 2). The difference between the 1977 GLOF discharge at reach N3 and the 1985 GLOF discharge at reach L5 and reach L7 becomes even greater if one takes into account that the 1977 GLOF discharge probably attenuated downstream from reach N3. Thus, the 1985 GLOF, which was larger in magnitude than the 1977 GLOF downstream from the Dudh Kosi and Bhoti Kosi confluence, either eroded, reworked, or buried the evidence of the 1977 GLOF below the Dudh Kosi and Bhoti Kosi confluence.

For the older GLOFs, the estimated GLOF discharges are seven to eight times greater than the SHFFs. Specifically, at the upper Bhoti Kosi reach, the estimated discharge of the GLOF was 400 m^3/s, approximately seven times greater than the SHFF at that location (Fig. 13; Table 6). For the upper Dudh Kosi reach, the estimated discharge of the GLOF was 700 m^3/s, approximately eight times greater than the SHFF at that location (Fig. 13; Table 6). The presence of the older GLOF deposits indicates that glacial-lake outburst floods are a recurring geomorphic process in the Mount Everest region.

6. Conclusions

The paleoflood hydrology techniques utilized in this study provided an effective means for assessing the hydrology of floods in the Mount Everest region of Nepal. Prior to this study, the flood hydrology of the 1977 and 1985 GLOFs and SHFFs in the Mount Everest region had not been established. A step-backwater model was used to construct the water-surface profiles of the GLOFs and SHFFs based on the geomorphic evidence of the GLOF and SHFF flood stages to estimate peak discharges. The upper surfaces of cobble and boulder bars, scour lines, and the lowest elevation of nonflooded surfaces were used to delineate the flood stage of the GLOFs. A white-gray silt-clay line along the channel margins (produced from glacier meltwater and snowmelt runoff) was used to define the water-surface elevation of the SHFFs. The most reliable GLOF and SHFF peak discharge estimates were upstream from constrictions where there was critical-depth control. Our assumption that flow was approaching critical flow during flow modeling provided a useful approach to reducing the uncertainty in selecting Manning's n values and estimating the peak discharges of the GLOFs and SHFFs along the high-gradient streams in this region.

The 1977 GLOF had an estimated peak discharge of 1900 and 1500 m^3/s at 8.6 and 11.5 km downstream from the breached moraine, respectively. The peak discharge of the 1985 GLOF ranged from 1375 to 2350 m^3/s, with the greatest peak discharge estimate occurring at the reach closest to the breached moraine at 7.1 km downstream from the breached moraine (reach L2) and the lowest peak discharge estimate occurring at the reach furthest from the breached moraine at 27 km downstream from the breached moraine (reach L8). The maximum discharges of the 1977 and 1985 GLOFs were probably larger at the breached moraines than the peak discharges estimate at reaches N1 and L2. The presence of older GLOF features along streams in other drainage basins indicate that extreme flooding from GLOFs is a recurring event in the Mount Everest region. The SHFF peak discharge estimates in the Mount Everest region ranged from 7 to 205 m^3/s and were positively correlated with increasing drainage area. The estimated SHFF discharges were 7 to 60 times less than the GLOF discharge estimates with lower ratios occurring furthest from the breached moraines because of the attenuation of the GLOFs as they progressed downstream and the increase in the SHFF discharges as contributing drainage area increased. The uncertainty of the GLOF and SHFF peak discharge estimates varied among the study reaches and ranged from -43% to 43% (Table 4) based on whether a conservative or liberal approach was used to evaluate the PSIs. Sensitivity analyses of the selected Manning's n and contraction/expansion coefficients in the step-backwater model indicate that the Manning's n coefficient had the greatest influence on the estimated discharges, whereas the contraction/expansion coefficients had only a minimal effect on the estimated peak discharges.

Acknowledgements

This project was funded for the most part by the National Science Foundation (Grant CMS-9320876). Additional funding was provided by the Geological Society of America, the Department of Earth Resources at Colorado State University (Chevron Research Grant), and the Lary Burns Memorial Scholarship. Many thanks are extended to Robert D. Jarrett for numerous comments, discussions, and insights about flow hydraulics and flow modeling of extreme floods in high-gradient streams. We acknowledge the thoughtful comments provided by David R. Butler and Richard A. Marston on an earlier version of the manuscript.

References

Ageta, Y., 1976. Characteristics of precipitation during monsoon season in Khumbu Himal. J. Jpn. Soc. Snow Ice 38, 84–88.

Arcement, G.J., Schneider, V.R., 1989. Guide for selecting manning's roughness coefficients for natural channels and floodplains. U. S. Geol. Surv. Water-Supply Pap. 2339. United States Government Printing Office, Washington D.C., pp. 1–38.

Bailey, J.F., Ray, H.A., 1966. Definition of stage-discharge relation in natural channels by step-backwater analysis. U. S. Geol. Surv. Water-Supply Pap. 1869A. United States Government Printing Office, Washington D.C., pp. 1–24.

Baker, V.R., 1978. Large-scale erosional and depositional features of the Channeled Scabland. In: Baker, V.R., Nummedal, D. (Eds.), The Channeled Scabland. National Aeronautics and Space Administration, Washington, DC, pp. 81–115.

Baker, V.R., 1984. Flood sedimentation in bedrock fluvial systems. In: Koster, E.H., Steel, R.J. (Eds.), Sedimentology of Gravels and Conglomerates. Can. Soc. Pet. Geol., Mem., vol. 10, Canadian Society of Petroleum Geologists, Calgary, Alberta, Canada, pp. 87–98.

Baker, V.R., 1987. Paleoflood hydrology and extraordinary flood events. J. Hydrol. 96, 79–99.

Benito, G., 1997. Energy expenditure and geomorphic work of the cataclysmic Missoula flooding in the Columbia River Gorge, USA. Earth Surf. Processes Landforms 22, 457–472.

Brower, B., 1991. Sherpa of Khumbu: People, Livestock, and Landscape. Oxford Univ. Press, Delhi, 202 pp.

Buchroithner, M.F., Jentsch, G., Wanivenhaus, B., 1982. Monitoring of recent geological events in the Khumbu area (Himalaya, Nepal) by digital processing of Landsat MSS data. Rock Mech. 15, 181–197.

Carling, P.A., 1987. Hydrodynamic interpretation of a boulder berm and associated debris-torrent deposits. Geomorphology 1, 53–67.

Cenderelli, D.A., 1998. Glacial-lake outburst floods in the Mount Everest region of Nepal: Flow processes, flow hydraulics, and geomorphic effects. Ph.D. Dissertation Colorado State University, Ft. Collins, 247 pp.

Cenderelli, D.A., Cluer, B., 1998. Depositional processes and sediment supply in resistant-boundary channels: examples from two case studies. In: Tinkler, K.J., Wohl, E.E. (Eds.), Rivers over Rock: Fluvial Processes in Bedrock Channels. American Geophysical Union Geophysical Monograph 107, Washington, DC, pp. 105–131.

Cenderelli, D.A., Wohl, E.E., 1998. Sedimentology and clast orientation of deposits produced by glacial-lake outburst floods in the Mount Everest region, Nepal. In: Kalvoda, J., Rosenfield, C.L. (Eds.), Geomorphological Hazards in High Mountain Areas. Kluwar Academic Publishers, The Netherlands, pp. 1–26.

Cenderelli, D.A., Wohl, E.E., in review. Flow hydraulics and geomorphic effects of glacial-lake outburst floods in the Mount Everest region of Nepal (submitted to Earth Surf. Processes Landforms).

Chow, V.T., 1959. Open-Channel Hydraulics. McGraw-Hill, New York, 677 pp.

Church, M., Jones, D., 1982. Channel bars in gravel-bed rivers. In: Hey, R.D., Bathurst, J.C., Thorne, C.R. (Eds.), Gravel-Bed Rivers. Wiley, New York, pp. 291–324.

Costa, J.E., 1983. Paleohydraulic reconstruction of flash-flood peaks from boulder deposits in the Colorado Front Range. Geol. Soc. Am. Bull. 94, 986–1004.

Davidian, J., 1984. Computation of water-surface profiles in open channels. U. S. Geol. Surv. Tech., Water-Resour. Invest., Book 3. United States Government Printing Office, Washington D.C., Chap. A15, 48 pp.

Ely, L.L., Baker, V.R., 1985. Reconstructing paleoflood hydrology with slackwater deposits, Verde River, Arizona. Phys. Geogr. 5, 103–126.

Fushimi, H., 1977. Glaciations in the Khumbu Himal (1). J. Jpn. Soc. Snow Ice 39, 60–67.

Fushimi, H., 1978. Glaciations in the Khumbu Himal (2). J. Jpn. Soc. Snow Ice 40, 71–77.

Fushimi, H., Ikegami, K., Higuchi, K., 1985. Nepal case study: catastrophic floods. In: Young, G.J. (Ed.), Techniques for Prediction of Runoff from Glacierized Areas. Int. Assoc. Hydrol. Sci. Publ., vol. 149, IAHS Press, Wallingford, Osfordshire, pp. 125–130.

Grant, G.E., 1997. Critical flow constrains flow hydraulics in mobile-bed streams: a new hypothesis. Water Resour. Res. 33, 349–358.

Grimm, M.M., Wohl, E.E., Jarrett, R.D., 1995. Coarse-sediment distribution as evidence of an elevation limit for flash flooding, Bear Creek, Colorado. Geomorphology 14, 199–210.

Hoggan, D.H., 1989. Computer-Assisted Floodplain Hydrology and Hydraulics. McGraw-Hill, New York, 518 pp.

House, P.K., Pearthree, P.A., 1995. A geomorphic and hydrologic evaluation of an extraordinary flood discharge estimate: Bronco Creek, Arizona. Water Resour. Res. 31, 3059–3073.

Hydrologic Engineering Center, 1995. HEC-RAS, River Analysis System, version 1.1, U. S. Army Corps of Engineers, Davis, CA.

Ives, J.D., 1986. Glacial Lake Outburst Floods and Risk Engineering in the Himalaya: A Review of the Langmoche Disaster, Khumbu Himal, 4 August 1985. International Centre for Integrated Mountain Development Occasional Paper No. 5, 42 pp.

Jarrett, R.D., 1984. Hydraulics of high-gradient streams. J. Hydraul. Eng. 110, 1519–1539.

Jarrett, R.D., 1987. Errors in slope-area computations of peak discharges in mountain streams. J. Hydrol. 96, 53–57.

Jarrett, R.D., 1990. Paleohydrologic techniques used to define the spatial occurrence of floods. Geomorphology 3, 181–195.

Jarrett, R.D., in review. Reliability of paleostage indicators and flood height used in paleoflood studies (submitted to Science).

Jarrett, R.D., Malde, H.E., 1987. Paleodischarge of the late Pleistocene Bonneville flood, Snake River, Idaho, computed from new evidence. Geol. Soc. Am. Bull. 99, 127–134.

Marcus, M.G., Roberts, K., Harvey, L., Tackman, G., 1992. An evaluation of methods for estimating Manning's *n* in small mountain streams. Mountain Res. Dev. 12, 227–239.

Mayewski, P.A., Jeschke, P.A., 1979. Himalayan and trans-

Himalayan glacier fluctuations since AD 1812. Arctic Alpine Res. 11, 267–287.

O'Connor, J.E., 1993. Hydrology, hydraulics, and geomorphology of the Bonneville flood. Geol. Soc. Am., Spec. Pap. 274, 83 pp.

O'Connor, J.E., Baker, V.R., 1992. Magnitudes and implications of peak discharges from glacial Lake Missoula. Geol. Soc. Am. Bull. 104, 267–279.

O'Connor, J.E., Webb, R.H., 1988. Hydraulic modeling for paleoflood analysis. In: Baker, V.R., Kochel, R.C., Patton, P.C. (Eds.), Flood Geomorphology. Wiley, New York, pp. 393–402.

O'Connor, J.E., Webb, R.H., Baker, V.R., 1986. Paleohydrology of pool-and-riffle pattern development: Boulder Creek, Utah. Geol. Soc. Am. Bull. 97, 410–420.

Rathburn, S.L., 1993. Pleistocene cataclysmic flooding along the Big Lost River, east central Idaho. Geomorphology 8, 305–319.

Stewart, J.E., LaMarche, V.C., 1967. Erosion and deposition produced by the flood of December 1964 on Coffee Creek Trinity County, California. U. S. Geol. Surv. Prof. Pap. 422K. United States Government Printing Office, Washington D.C., pp. 1–22.

Tinkler, K., 1996. Critical flow in rockbed streams with estimated values of Manning's *n*. Geomorphology 20, 147–164.

Trieste, D.J., 1992. Evaluation of supercritical/subcritical flows in high-gradient channel. J. Hydraul. Eng. 118, 1107–1118.

Trieste, D.J., Jarrett, R.D., 1987. Roughness coefficients of large floods. In: James, L.G., English, M.J. (Eds.), Irrigation and Drainage Division Specialty Conference, Irrigation Systems for the 21st Century, Portland, Oregon, Proceedings. Am. Soc. Civ. Eng., New York, pp. 32–40.

Vuichard, D., 1986. Geological and petrographical investigations for the mountain hazards project, Khumbu Himal, Nepal. Mountain Res. Dev. 6, 41–52.

Vuichard, D., Zimmermann, M., 1986. The Langmoche flash-flood, Khumbu Himal, Nepal. Mountain Res. Dev. 6, 90–94.

Vuichard, D., Zimmermann, M., 1987. The 1985 catastrophic drainage of a moraine-dammed lake, Khumbu Himal, Nepal: Cause and consequences. Mountain Res. Dev. 7, 91–110.

Waythomas, C.F., Walder, J.S., McGimsey, R.G., Neal, C.A., 1996. A catastrophic flood caused by drainage of a caldera lake at Aniakchak Volcano, Alaska, and implications for volcanic hazards assessment. Geol. Soc. Am. Bull. 108, 861–871.

Webb, R.H., O'Connor, J.E., Baker, V.R., 1988. Paleohydrologic reconstruction of flood frequency on the Escalante River, south-central Utah. In: Baker, V.R., Kochel, R.C., Patton, P.C. (Eds.), Flood Geomorphology. Wiley, New York, pp. 403–418.

Wohl, E.E., 1992a. Bedrock benches and boulder bars: Floods in the Burdekin Gorge of Australia. Geol. Soc. Am. Bull. 104, 770–778.

Wohl, E.E., 1992b. Gradient irregularity in the Herbert Gorge of northeastern Australia. Earth Surf. Processes Landforms 17, 69–84.

Wohl, E.E., 1995. Estimating flood magnitude in ungauged mountain channels, Nepal. Mountain Res. Dev. 15, 69–76.

Wohl, E.E., 1998. Uncertainty in flood estimates associated with roughness coefficient. J. Hydraul. Eng. 124, 219–223.

Zimmermann, M., Bichsel, M., Kienholz, H., 1986. Mountain hazards mapping in the Khumbu Himal, Nepal, with Prototype Map, scale 1:50,000. Mountain Res. Dev. 6, 29–40.